Controller Design for Active Vibration Damping with Inertial Actuators

by

Jason Qi Chen Zeng

A thesis
presented to the University of Waterloo
in fulfillment of the
thesis requirement for the degree of
Masters in Applied Science
in
Mechanical and Mechatronics Engineering

Waterloo, Ontario, Canada, 2019

AUTHOR'S DECLARATION

I hereby declare that I am the sole author of this thesis. This is a true copy of the thesis, including any required final revisions, as accepted by my examiners.

I understand that my thesis may be made electronically available to the public.

Abstract

In the machining industry, there is a constant need to improve productivity while maintaining required dimensional tolerances and surface quality. The self-excited vibration called chatter is one of the main factors limiting machining productivity. Chatter produces unstable cutting conditions during machining and unstable forces will damage and shorten the life of the machine tool. It can also damage the cutting tool, machining components as well as produce a poor surface finish on the workpiece. Researchers have developed various chatter suppression techniques such as changing process parameters, spindle speeds, and using passive dampers. However, many of these methods are not very robust to changing dynamics in the machine tool due to changing machine positioning, cutting setups, etc. Active vibration damping with a force actuator is a robust method of adding damping by due to its bandwidth and variable controller gains. However, the commissioning of the controller design for the actuators is not trivial and requires significant manual tuning to reach optimal productivity. The research presented in this thesis aims to simplify and automate the controller design process for force actuators.

A frequency domain, sensitivity based automatic controller tuning method for force actuators has been developed. This method uses the measured actuator dynamics and open-loop system dynamics to develop a prediction tool for closed-loop responses without needing to have the complete system model (model free). By monitoring the predicted closed-loop response of various virtually designed controllers, an optimal controller is found amongst the candidate parameter values. The stability of the system and actuator is monitored during the search to ensure that the system is stable throughout its bandwidth that the actuator does not become saturated. The controller is then experimentally tested to ensure that the predicted output is the same as the real output.

In cases where the system has several vibration modes that are in counter-phase and close in frequency, the model-free approach does not perform well. A more complex model-based control law has also been developed and implemented. The method automatically identifies a transfer function model for the measured open-loop system dynamics and synthesizes mixed-sensitivity optimization based controller to damp out the modes in counter-phase.

In order to verify that the model-based controllers can reduce vibration modes in counter-phase, a small-scale experimental setup was developed to mimic machine tools with vibration modes in counter-phase. A flexure was designed and fabricated. A shaker from Modal Shop is used as an active

damping actuator to reduce the flexure's vibration modes. It was concluded that while the model-based controller synthesis techniques were able to damp the vibration modes in counter phase, the flexure was too simplistic and the model-free controller was able to achieve similar results.

Acknowledgements

Foremost, I would like to thank my supervisor Professor Kaan Erkorkmaz and Dr. Xavier Beudaert for their support, ideas and enthusiasm during my studies. Their knowledge and support have been pivotal in the development of my research at University of Waterloo.

I would like to thank IK-4 Ideko who has graciously sponsored this project and whom have provided the vital equipment necessary in order to carry out the experimental validation and knowledge resources to carry out further theory development. I would especially like to thank Dr. Jokin Munoa, Dr. Iker Mancisidor, Alex Peña Sevillano, Iñaki Laka, Jérôme Loch, Oier Franco and everyone else who have helped me during my stay at IK4-Ideko.

I would also like to thank the University of Waterloo MME technical staff Robert Wagner, Neil Griffith, James Merli and Jason Benninger for their help in the design, manufacturing and setup of experimental equipment.

Finally, I would like to thank all my colleagues from the Precision Control Laboratory, especially Hessam Kalbasi and Ahmet Okyay for sharing their knowledge on equipment and theory, my friends and my family for their support during my studies.

Dedication

To my family.

Table of Contents

List of Figures

List of Tables

Chapter 1
Introduction

Metal cutting is one of the most popular methods of manufacturing to shape metal components. The process involves a cutting tool and a workpiece material mounted on a machine tool. The cutter is fed into the workpiece and material is removed by a cutting edge of the tool. The cutting process generates forces that lead to vibrations within the machining setup (tool, machine structure, fixture, etc.). The vibrations can produce instability within the machining process [1]. The unstable vibrations are called chatter vibrations, which shortens the life of the tools and machine components, prohibits good surface quality and ultimately hinders productivity. Machine tool builders such as Soraluce Inc. have sensors within the machine tool in order to measure the cutting forces and disturbance vibrations. They have also embedded force actuators within machines to minimize the chatter vibrations and improve machine productivity [2].

1.1 Thesis Objectives

The objective of this thesis is to conduct research to synthesize controllers for active vibration damping via force actuators to improve productivity in the field of machining. The goal is to create a rapidly deployable tool for engineers to quickly commission active damping actuators faster embedded within custom machining centers and workpieces.

1.2 Thesis Layout

In Chapter 2, a literature review is conducted on existing research in machining and vibration damping of machine tools. Researchers have developed hardware and control techniques in order to damp out chatter vibrations originating from the structures of the machine tools. However, there is a lack of automation techniques for commissioning the controllers and a highly trained engineer is required to manually tune the controllers [3].

In Chapter 3, the structural identification method is introduced. In order to carry out vibration damping and improve process performance, information about the system must be obtained and analyzed. The most popular way of understanding the system is looking at the frequency response function (FRF). In order to obtain the FRF, the system needs to be excited across a frequency spectrum and its response captured. The setup uses an electromagnetic actuator, computer and transducer to capture the system response due to acting force.

In Chapter 4, an automatic method of controller parameter tuning is presented. This approach saves engineering time to tune the controller for each system and differing use case. It uses a model free frequency domain approach. The algorithm computes a range of user-defined controller parameter values and makes a prediction of the closed-loop system response. The prediction is evaluated on its stability and performance in the sensitivity function and overall vibration damping. The overall controller with the best vibration damping performance is selected. Testing the method on different structures show that the experimental results and predictions align closely with each other.

In Chapter 5, a least squares based curve-fitting algorithm is described. The algorithm is created in order to extract system parameters and to create a mathematical model for model-based controller design. The model is comprised of a series of 2^{nd} order systems. The newly developed method is compared against the existing MATLAB transfer function identification and it shows improvements in the fit quality in certain situations.

In Chapter 6, a flexure mimicking the dynamics of a milling machine is developed to develop and test model-based controllers. In Chapter 4, it is shown that there are situations where a model-free controller can fail. This is the case in systems with non-collocated control where the actuation and sensing points are at different locations and cause counter-phase vibration modes. A flexure is designed using computer simulations and its properties are verified after fabrication using hammer testing. The experimental results verified the simulations and the flexure exhibits counter-phase vibration mode properties. The flexure dynamics are found to be too simple and the controller design used in Chapter 4 is able to suppress the flexure dynamics.

In Chapter 7, $\mathcal{H}_\infty$ and $\mathcal{H}_2$ model-based controllers are introduced to suppress vibrations while avoiding counter-phase modes. $\mathcal{H}_\infty$ and $\mathcal{H}_2$ controllers guarantees the stability of the system while minimizing the system disturbance and overall disturbances, respectively. The simulations and experimental results of the $\mathcal{H}_\infty$ and $\mathcal{H}_2$ controllers match closely with each other and are shown to minimize the greatest peak and overall of the system disturbances, respectively.

Chapter 2
Literature Review

2.1 Introduction

In metal cutting manufacturing processes, increasing the material removal rate while maintaining good surface quality, longevity of tools and machine components will increase overall productivity. However, the vibration phenomenon known as chatter limits metal cutting productivity by creating instabilities in machining processes [1] [4]. Chatter is an important problem today in the manufacturing field and still will be in the future because of the following reasons:

- Faster and more powerful tooling will increase both material removal rate and the risk of machining vibrations
- Inaccurate prediction of damping in machine design phase leads to unforeseen vibration problems
- Low friction guided systems used for accuracy have poor damping
- Light weight machine designs intended to be eco-friendly and faster but more prone to vibrations
- Manufacturing of new flexible parts that are light in mass and less stiff leads to vibration problems

There has been substantial research on the suppression of chatter vibrations. These methods include spindle speed variation, process planning using stability lobe diagram, special tool geometries, redesign of the system to include more stiffness, inclusion of flexures to increase stiffness, passive dampers to active dampers [2]. However, many of these methods work for only one machining configuration and require individual analysis and modifications for changing machine and cutting configurations. An active damping system has a wide bandwidth and a controllable output that is adaptable to the different variations of machining configurations and cutting positions of a machining tool [5].

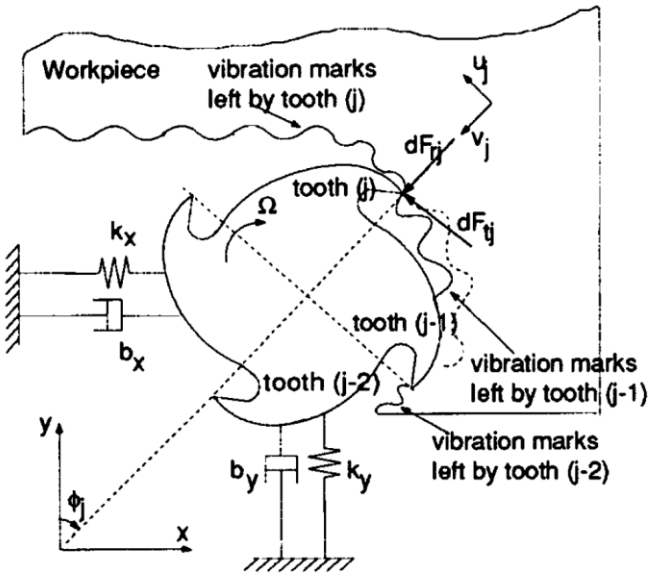

Figure 2-1 2D schematics of milling [6]

2.2 Chatter Vibrations

Self-excited vibrations named chatter occurs in machining processes and limits the productivity. Initially, one of the structure modes of the machine tool structure, spindle, tool, workpiece, workpiece fixture is excited from forces generated in the cutting process. The dynamic flexibilities of the system are displayed in Figure 2-1. The excited structural mode creates a wavy surface on the machined face, and another wavy surface is created on the successive passing cut. Tobias [7] and Tlusty [8] first referred to this as the regenerative effect of chip thickness in metal machining. The wavy cuts can be observed in Figure 2-1. From the figure, two successive machining cuts produce wavy surfaces that are out of sync. The wavy surfaces can be also be observed as two sinusoidal waves with a phase shift. This phase shift can cause the difference between the amplitude (maximum chip thickness) to grow exponentially while oscillating at a frequency that is close to one of the system structural modes. The growing chip thickness will lead to vibrations due to the extra force required to cut the thicker chips. The vibrations cause uneven and poor surface finishes on workpieces. They also shorten the work-life of tools and mechanical components of the machine due to the high resultant forces generated. The effects of chatter on different workpieces and cutting processes can be seen in Figure 2-2.

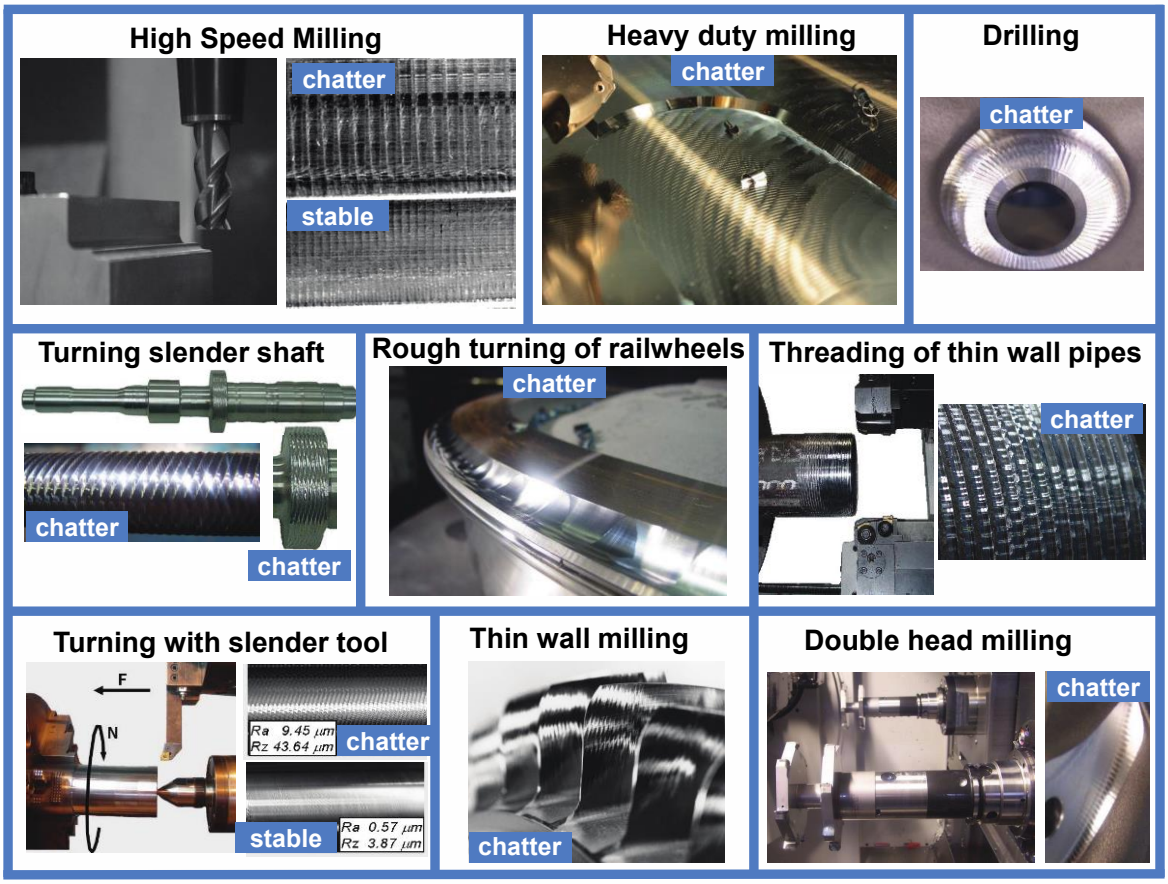

Figure 2-2 Examples of chatter appearing in different machining applications [1]

Chatter vibrations can originate from any part of the machining process that possesses dynamic flexibility. Some of the most common flexibilities in machine tools come from the bending of the spindle, the cutting tool, the column or ram of the milling head, workpiece fixture or the workpiece itself. The different flexibilities are illustrated in Figure 2-3. In large scale machining centers such as the one seen in Figure 2-3, chatter problems arise in the low frequency ranges from 20 to 200 Hz. These chatter problems are caused by the structural modes of the heavy components of the machine tool [5]. Chatter problems in the high frequency range from 0.5 to 10 kHz are caused by the flexibility of the tool and spindle [9]. The low frequency dynamic properties are subject to change if the machine changes its position, or if cutting orientations change. An example of changing dynamics would be the ram overhang of the machine in Figure 2-3 extending or retracting. As the ram extends outwards, its flexibility increases as its dynamic behavior is similar to a cantilever beam.

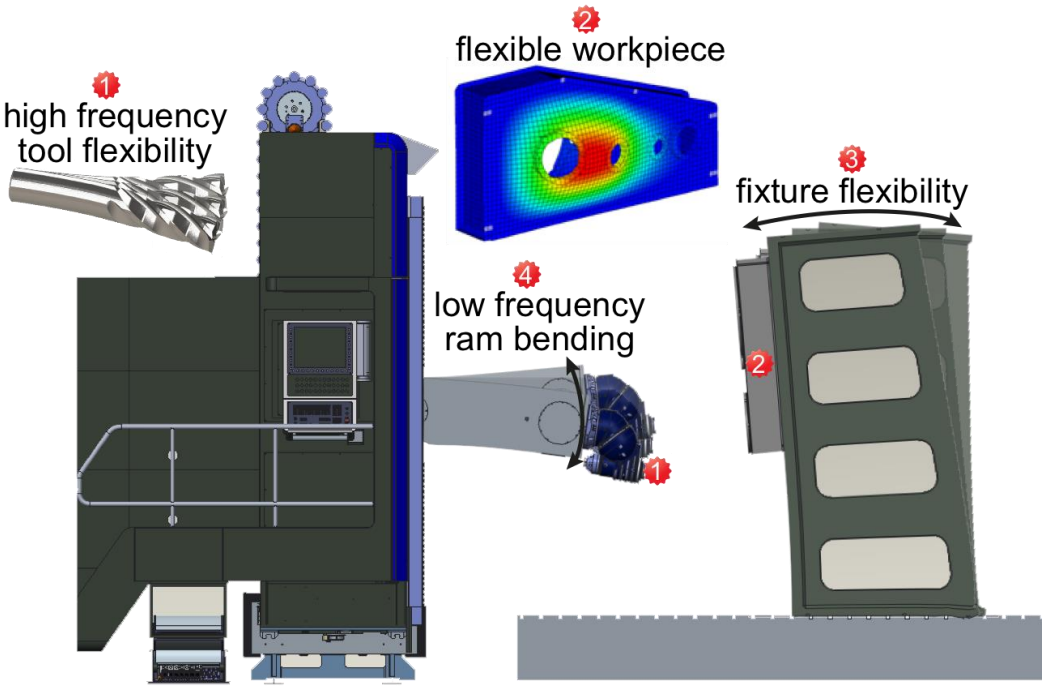

Figure 2-3 Flexible structural modes of ram type milling system [1]

2.2 Chatter Suppression Techniques

There are many approaches to solving the problem of chatter within machining operations. Process planning methods such as spindle speed variation and stability lobe diagrams do not require the addition of any hardware components to the machine tool setup. Instead, the parameters of the machine or manufacturing method are studied and optimized to avoid the chatter vibration problems. Passive and active damping methods introduce additional components to the machine tool or workpiece to alter the damping of the system to reduce vibrations. These various techniques will be introduced and explained in the following sections.

2.2.1 Stability Lobe Diagram

A stability lobe diagram (SLD) is used to alter the depth of cut (a) and spindle speed (n) of a machining process to avoid excitation the vibration modes of a machine tool [10]. SLDs display the combinations of depth of cuts and spindle speeds that will cause unstable conditions of cutting. Altintas and Budak [11] developed SLDs for metal milling. A SLD is synthesized by using the cutting coefficients, system dynamic parameters, process parameters and the tool geometry [6] [12]. The required information and a SLD can be seen in Figure 2-4. The grey region represents the unstable combinations of spindle speed and

depth of cut and the white region represent the stable combinations. The machining process can then use the stable depth of cut and spindle speed parameters to avoid chatter vibrations. One main limitation of the SLD technique is that the performance is inadequate in machine tools and processes where multiple vibration modes are present [13].

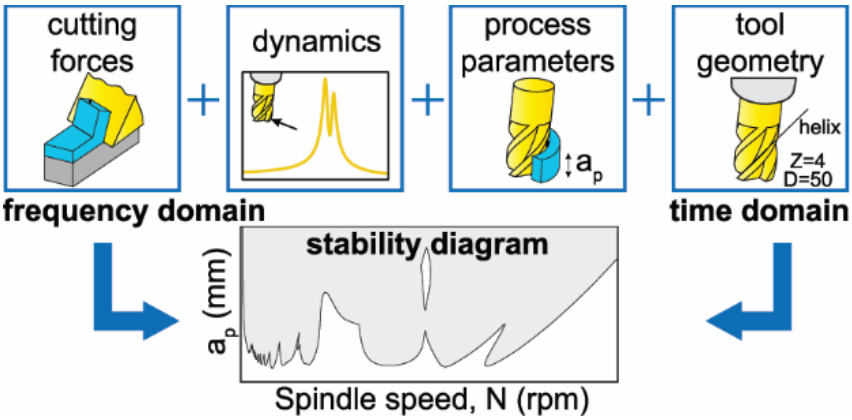

Figure 2-4 Stability lobe diagram generation [2]

2.2.2 Spindle Speed Variation

The chatter problem during machining is a build up from the regenerative effect. By using varying the speed of the cutter, a time delay is introduced that can separates the successive wavy cuts of the regenerative effect. Altintas and Chan [14] were able to develop a chatter detection and spindle speed variation method to interfere the period between each layer of cut and minimize the regenerative effect. This method has been successfully implemented in low spindle speed milling [15], turning [16] and grinding processes [17]. However, this method faces challenges when there are flexible components (low damping) within the system and when the cutting process is highly unstable. The surface finish of the workpiece will still be poor for highly accurate requirements [18].

2.2.3 Passive Damping

Damping is a way of describing the mechanical energy dissipation characteristic of a component [2]. Passive dampers increase the damping of the system modes without the need of electronic hardware or computer control. Passive dampers are relatively straightforward to design and implement. The passive damper adds damping to the system by tuning its mass, spring (k) and damping (c) coefficients to match the resonant frequency (ω_n) of the target system vibration mode. The overall damping of the system is increased by the additional damping of the passive damper and the resonant peak of the vibration mode is

reduced. Figure 2-5 shows the response of the system before and after the addition of a passive damper. The most popular passive dampers are the vibration absorber and the tuned mass damper (TMD) as seen in Figure 2-5 [19]. The disadvantages of passive dampers is that it needs to be retuned if the target resonance of the system changes in frequency and that the passive damper would not work in systems with multiple vibration modes. Semi-active passive dampers have been developed with an adjustable damper and spring to improve robustness of the passive dampers. However, the bandwidth of passive dampers is insufficient for use in system with a wide frequency range and the speed of adjustment is not fast enough for rapidly changing system dynamics.

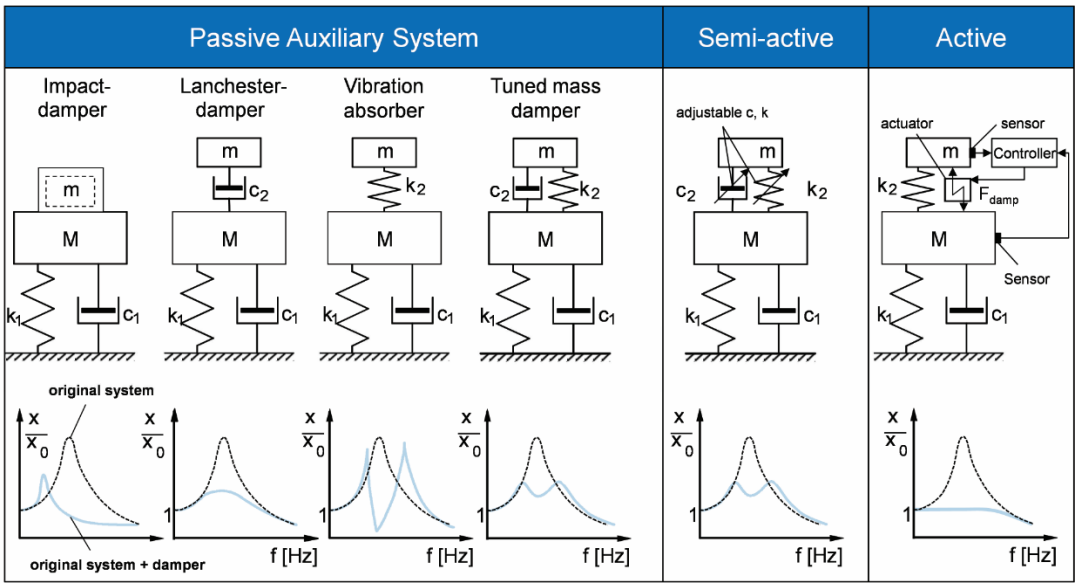

Figure 2-5 Types of passive damper systems [19]

2.2.4 Active Vibration Damping

Active vibration damping techniques provides a robust solution when the system dynamics change frequently and when a range of vibration modes need to be damped. Active damping techniques involves the real time monitoring of vibrations and using the data obtained from monitoring to generate a controlled force by an actuator to minimize the effect of vibrations. The most popular actuators used for active vibration damping are piezoelectric and electromagnetic actuators [13]. Mancisidor et al [5] were able to mount a biaxial electromagnetic actuator on the column ram of a Soraluce machining tool and successfully add damping to the system. However, the closed-loop controller of the actuator needs to be carefully designed to avoid creating instability [19].

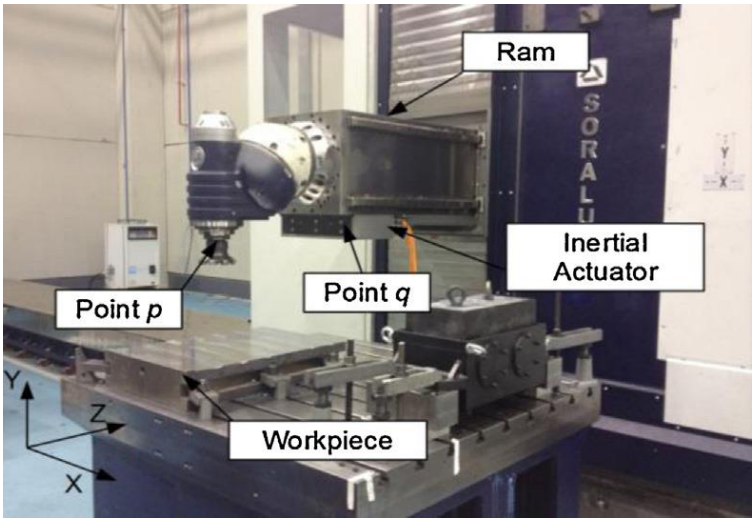

Figure 2-6 Ram type milling machine with active damper [5]

2.2.4.1 Active Damping Control Law

One of the most effective feedback control laws to damp vibration modes using an actuator is direct velocity feedback. The direct velocity feedback (DVF) law involves using the negative feedback of the measured velocity of the structure to damp vibrations. Accelerometers mounted on the structure monitors the structural vibrations and the acceleration signal is integrated to produce the velocity signal. DVF has been previously implemented on several active dampers to suppress vibrations with in machine tools [5] [20] [21]. The basis of DVF will be explained in the following section.

The overall dynamics of a structure can be defined by Eqn. (2.1).

$$m \cdot \ddot{x}(t) + c \cdot \dot{x}(t) + k \cdot x(t) = F_d(t) + F_{act}(t) \tag{2.1}$$

where m, c, and k are modal mass, damping and stiffness respectively and F_d and F_{act} are the disturbance and actuator forces respectively. The actuator force is as follows:

$$F_{act}(t) = -G \cdot \dot{x}(t) \tag{2.2}$$

where G is the selected gain and additional filters that the user sets and is multiplied by the sensed velocity signal which comes from the integration of acceleration signal.

$$m \cdot \ddot{x}(t) + \underbrace{(c + G)}_{\text{additional damping introduced}} \cdot \dot{x}(t) + k \cdot x(t) = F_d(t) \tag{2.3}$$

As one can see from Eqn. (2.3), the DVF control law increases the damping within the structure by using an actuator with closed-loop controls. This control law applicable to manufacturing processes where machine tool structures and workpieces that require additional vibration damping.

2.2.5 Closed-loop Response Prediction

The closed-loop response can be predicted by creating a model from the collected open-loop, closed-loop measurements and the controller structure. This allows the closed-loop response to be monitored virtually and allows a faster tuning of the controller response. The comparison between the closed-loop prediction and experiment results can be seen in Figure 2-7.

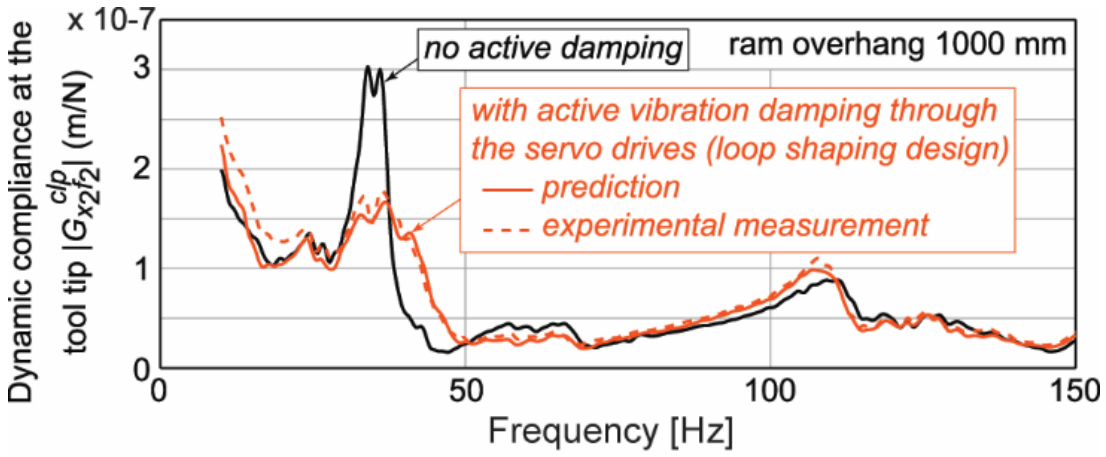

Figure 2-7 Prediction of closed-loop response [3]

2.3 Autotuning

There has been some research conducted about automated system identification of machine tools and auto-tuning of the vibration damping controller. Zaeh and Kleinwort [22] were able to develop an auto-tuning method using an actuator to excite the machine tool structure for identification and vibration damping purposes. A direct velocity feedback (DVF) and $\mathcal{H}_\infty$ controller were implemented to damp the most flexible vibration mode in the machine tool by the same actuator used for system identification. However, there is currently no work done for tuning the controller to damp multiple vibration modes within the machine tool. As well in the automatic controller design presented, there were no analysis conducted on the closed-loop sensitivities and stability. Their results can be found in Figure 2-8.

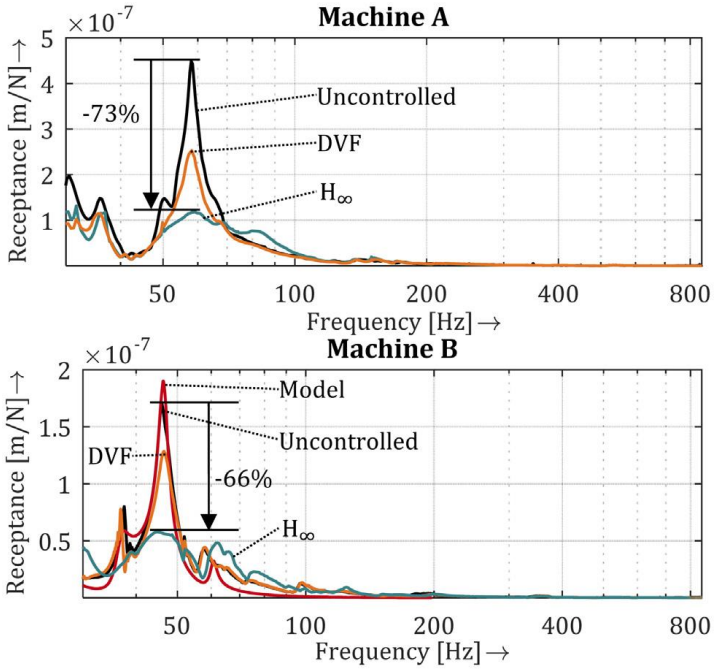

Figure 2-8 Damping on Machine A: SPINNER U5-620 and Machine B: PITTLER PV630 [22]

2.4 Model-Based Controls

There have also been studies and research conducted in the field of model-based controls for vibration damping. Model-based controllers can be used in systems that exhibit counter-phase mode behavior in non-collocated control [8]. An example displaying the effects of counter-phase modes can be seen in Figure 2-9, one vibration mode is suppressed while two other modes are destabilized when closed-loop feedback is activated. The closed-loop controller in Figure 2-9 is a model-free controller. Research has been conducted using LQG and $\mathcal{H}_\infty$ controllers to damp vibration modes by synthesizing controllers that penalize the area underneath the FRF and highest FRF peak, respectively [7]. It has been demonstrated that mixed sensitivity $\mathcal{H}_\infty$ control can increase damping and reject output disturbance in electric power systems [23] [24].

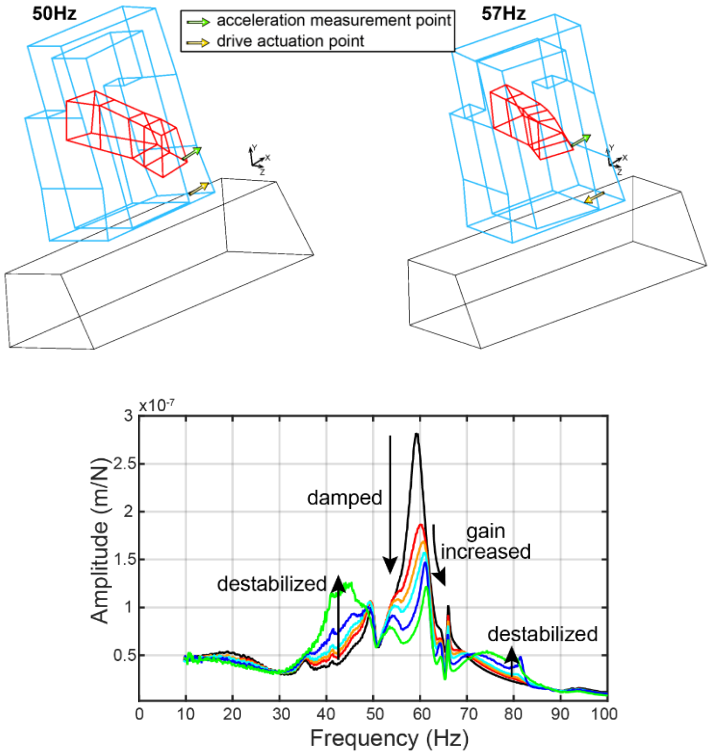

Figure 2-9 Counter-phase vibration modes in machine tool [25]

2.5 Conclusion

In this chapter, the importance of understanding and eliminating chatter vibrations in the machining industry have been discussed. Several different methods of chatter vibration suppression has been explained. Active damping is a robust method of eliminating chatter vibrations originating from several vibration modes and changing machining dynamics due to changing machine configurations. However, the time it takes to tune and deploy a controller for each machining configuration is substantial. There has been some work done in the automatic system identification and controller design field but improvements can be done. The research conducted in this thesis discusses about methods to automatically design controllers for active damping that helps engineers to quickly deploy and tune controllers.

Chapter 3
Structure Identification

3.1 Introduction

In machining processes, disturbances in the form of vibrations occur within the machine structure. These vibrations hinder the productivity of the machining process as well as decrease the tool life. Thus, it is important to have a method of analyzing the behavior of the system due to disturbances. In this chapter, the method of identifying the structural dynamics is presented. The measurement setup structure is explained in Section 3.3. The actuator excitation and measurement method is explained in Section 3.4.

3.2 Modal Testing

Modal testing is the process of testing components or structures in order to obtain a mathematical understanding of their dynamic behavior [26]. The most important analysis is to observe how the structure responds under certain excitation conditions. The excitation is typically a force applied at one point or multiple points on the structure via an actuator. A sensor, typically an accelerometer, measures the output. The output to input ratio is displayed as a frequency response function (FRF). The FRF displays the magnitude of displacement of the system across the frequency range. A machine tool structure or workpiece can be modeled by a series of mass spring damper systems as seen in Figure 3-1. Each individual mass spring damper system has a certain excitation frequency and damping ratio which are displayed from the FRF.

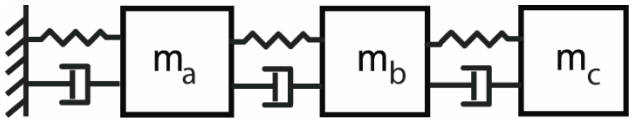

Figure 3-1 Model schematic

3.3 Measurement Setup

The key instrumentation items for measuring the FRF of a mechanical system can be simplified down to three components:

- An excitation actuator
- Transducers for measuring the physical outputs
- An analyzer to extract the desired information

A schematic of the measurement cycle can be seen in Figure 3-2. The measurement cycle process is controlled from the workstation computer. The workstation computer will start the measurement cycle by sending an excitation signal to the controller hardware. The controller hardware will transfer the control signal to the linear power amplifier to convert the electrical control signal into current. The current will power the actuator and induce an inertial force onto the structure. Transducers mounted onto the structure captures the system response and the measurement data is captured by the data acquisition device (DAQ). The FRF of the system is obtained by performing the Fourier transform on the measured input and output signals.

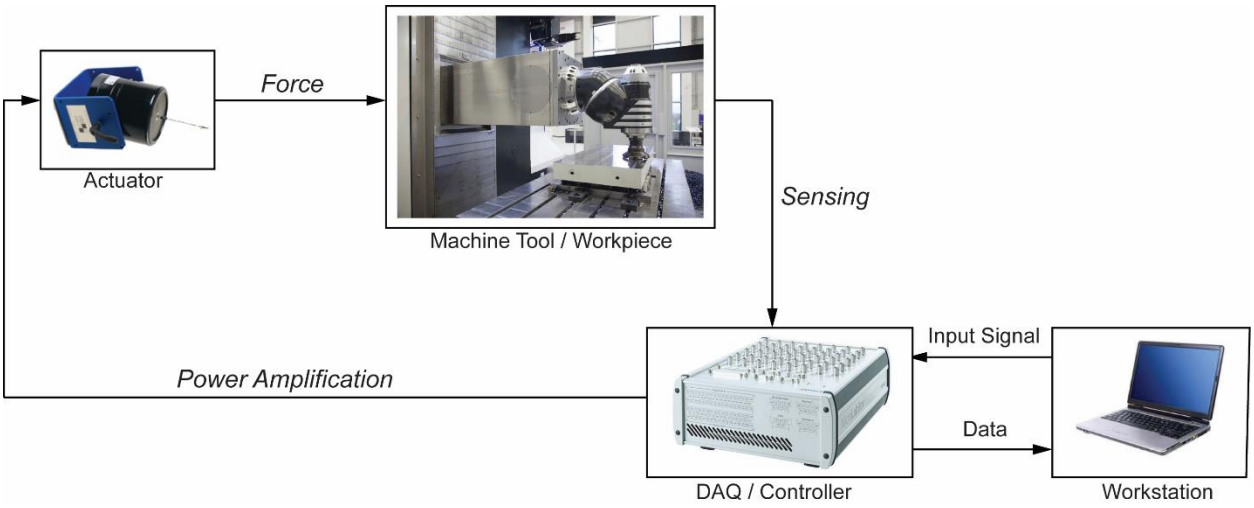

Figure 3-2 Hardware schematic for measurement setup

3.4 Actuator Excitation

Electromagnetic shaker actuators can be used to excite a structure of interest. The shakers induce a controlled inertial force onto the structure. The excitation signal can vary in frequency range, length and the force. The shaker excels at exciting larger structures where greater force and longer duration of excitation are required to fully excite the structural modes. One main disadvantage is that more complicated instrumentation and power equipment is required in order to power and control the shaker. More setup time is required as well in order to mount the shaker at the desired position [26].

The shaker uses the concept of the Lorentz force in which a moving mass is placed inside an alternating magnetic coil. The electrical excitation control signal is converted into current via an amplifier. The current travels through wound coils that will induce a magnetic field [13]. The magnetic field then moves the charged moving mass, generating an inertial force. An example actuator is shown in Figure 3-3.

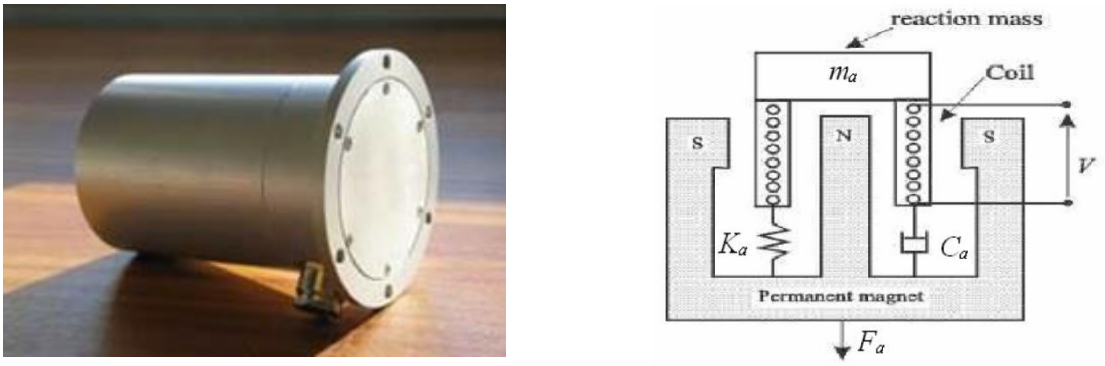

Figure 3-3 Micromega Dynamics active damping actuator [27]

3.4.1 Excitation Signal

There are two types of excitation signals that are used for conducting model identification of the structure, chirp, sinestream signals. The two signals are sinusoidal in nature and vary in frequency over time. This way, all of the structural vibration modes can be captured on the FRF within the frequency range of the excitation. The chirp signal is a sinusoidal signal that varies in frequency as time increases. It can go from low frequency to high frequency or vice versa over specified time duration. The sinestream signal is a sinusoidal signal that contains a series of sinusoids at difference frequencies and lasts for a specified duration period for each frequency value.

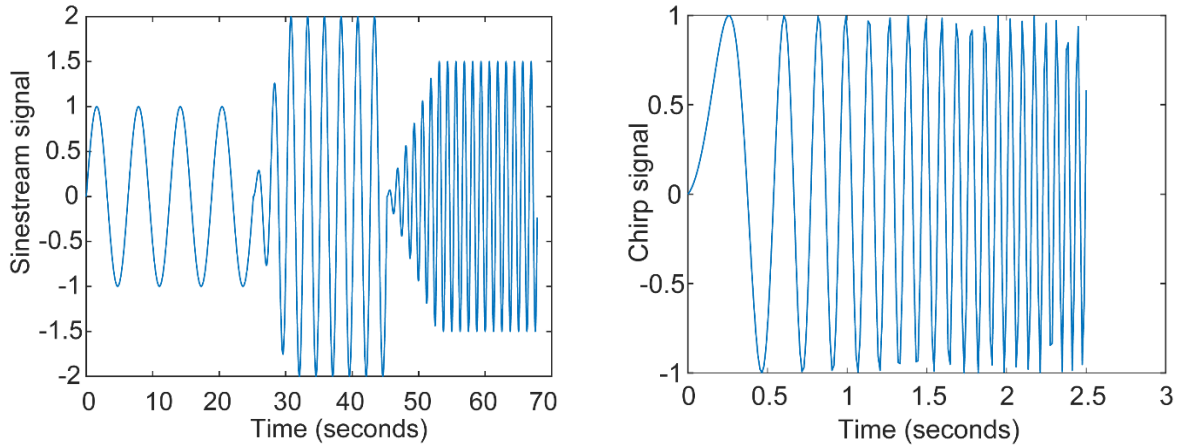

Figure 3-4 Sinestream (left) and chirp (right) time domain signal

The two different excitation signals are very similar upon definition, however in Figure 3-4 the differences can be observed. The chirp signals quickly traverses through the specified frequency band without a stop between each frequency step. This could lead to inaccurate FRFs as one vibration mode is excited at one frequency step and the excited mode does not settle within the time the next frequency step

is executed. This can lead to cross interference within the FRF. While the sinestream signal takes longer to conduct, it generates a cleaner FRF due to the ability to specify the number of excitation signal periods at each frequency step. This will allow any vibrations from previous frequency steps to die out and not cross contaminate. Thus, the sinestream excitation signal will be used to conduct any structural identification that needs precision such as model identification.

3.4.2 Actuator Excitation FRF Construction

The system response in proper units needs to be constructed. In vibration research the FRF magnitude is in units of displacement over force. This gives a better understanding of the system behavior due to disturbance forces. Currently the input signal is measured in voltage and the output signal is measured in acceleration. The actuator output force is measured with the use of a dynamometer. The measurement setup can be seen in Figure 3-5. The setup consists of the damping actuator mounted on top of a Kistler dynamometer. A frequency sweep is conducted the actuator mounted on the dynamometer and the input voltage signal (V) is captured with the output force signal (N). Thus, an actuator force model can be constructed (N/V). With the actuator force model obtained, the FRF can be constructed by dividing the initial displacement response (m/V) by the actuator force model (N/V) to achieve the desired FRF units of (m/N).

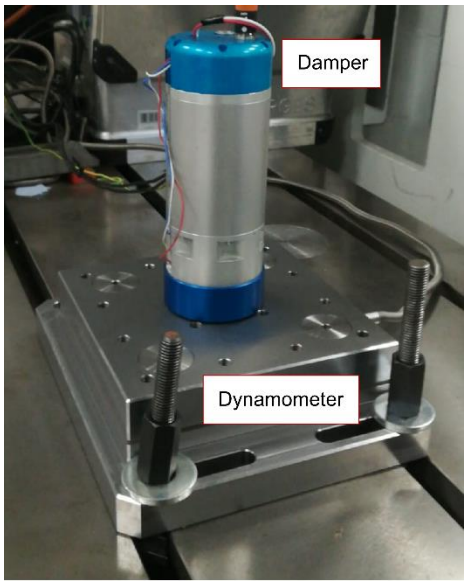

Figure 3-5 Damper force measurement setup

The process of converting the FRF is seen in Figure 3-6. The experimentally obtained FRF is transformed by the measured actuator dynamics (F/V) to obtain the receptance FRF.

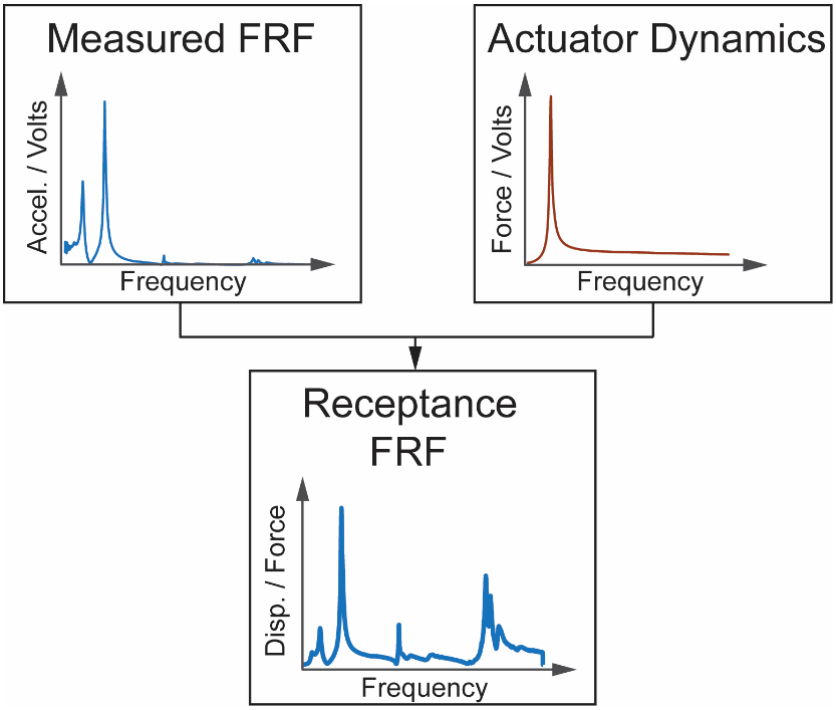

Figure 3-6 Calculation of FRF

3.5 Hammer Excitation

In impact hammer testing, an instantaneous impact is applied to the structural system. The force of the impact will excite the system into vibration and its response will be captured by a transducer. The time-domain signals of the impact force and the system response are both measured and recorded. Then the FRF is built by transforming the time-domain signals into the frequency domain through the use of Fourier transform. An example of impact hammer testing can be seen in Figure 3-7.

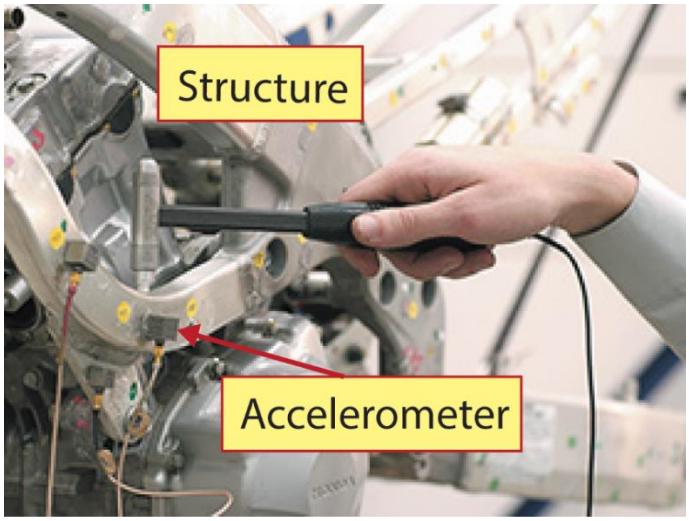

Figure 3-7 Hammer impact testing [28]

The impact hammer testing is good for obtaining a FRF of a system quickly and easily. However, there are times impact testing does not function well. For example, when the structure is very large, the impact force of the hammer may not excite all of the modes of the structure. Hence, shaker actuators are better for obtaining the FRF for large structures.

3.6 Conclusion

In this chapter, the method of obtaining the structural frequency response is presented. It is used to analyze the system and to aid engineers in adjusting the actuator controller to control the system to desired performance levels. The frequency response is obtained using an excitation force actuator and an accelerometer transducer. Two different excitation signals are introduced and compared with the sinestream as the more accurate excitation signal over the chirp signal. A mathematical recalculation is performed to transform the FRF magnitude values into displacement over force. The structural identification method will be used obtain the frequency response of the machine tool and structures when a damping actuator is used.

Chapter 4
Frequency Domain Based Automatic Controller Tuning

4.1 Introduction

Electromagnetic actuators can be mounted to the machine tool structure to conduct structural identification. The actuators can also be used as vibration dampers to suppress disturbance vibrations that occur during the machining process. In this chapter, the controller design for the vibration damping actuator is presented. Section 4.2 explains how to use actuators as a vibration damper. Section 4.3 introduces the vibration damping control law and the filters used. Section 4.4 describes a virtual tool that has been developed to automatically tune the controller to obtain optimal vibration damping. The method is tested and the results are analyzed in Section 4.5. Section 4.6 talks about some of the drawbacks of using this approach.

4.2 Vibration Damping Actuator

Vibration damping actuators can be mounted on a machine tool structure to suppress chatter vibrations that appear during a metal cutting process. This can be implemented on both the machine tool and on the workpieces itself. Figure 4-1 depicts an actuator mounted externally on a workpiece and internally on a machine tool ram respectively.

Figure 4-1 Actuators used for vibration damping

Feedback control strategies are implemented to suppress the vibrations in the structures. Sensors such as accelerometers mounted on the structure monitor the structure's vibrations and convert the vibrations into electrical signals that are sent to a monitoring system. The monitoring system analyzes the vibration signals and calculates the damping force signal from a controller. The damping force signal is then sent to

the electromagnetic actuator to produce a damping force on the structure. A figure depicting this process can be seen in Figure 4-2. An actuator is embedded into the ram of the milling machine. An accelerometer measures the disturbance forces during the machining process. The controller takes measured signals and calculates a force to suppress the disturbance forces to the value of the reference (zero).

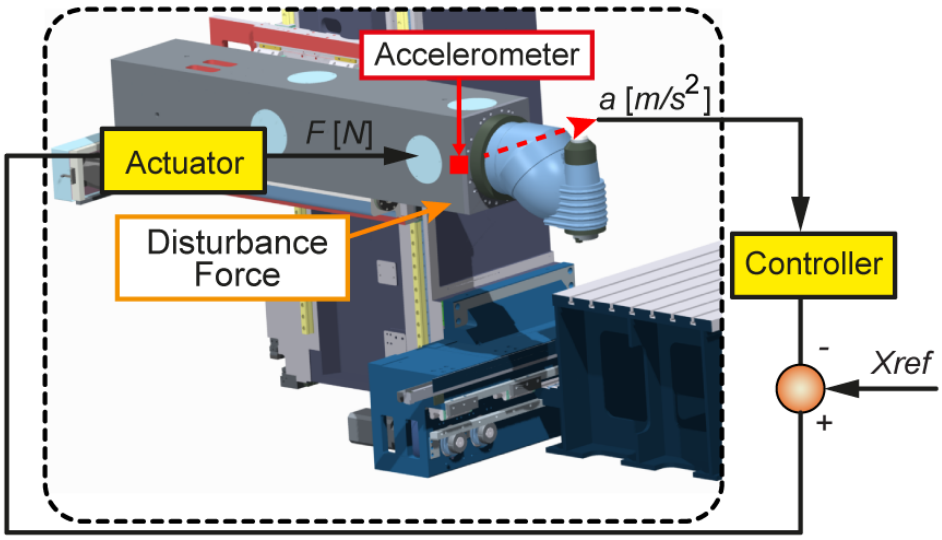

Figure 4-2 DVF closed-loop feedback control

4.3 Control Law

The control law strategy need to be designed properly in order to successfully damp out the disturbance vibrations. The controller also needs to avoid making the system unstable, saturating the actuator and amplifying noise. A set of filters will need to be designed in order to achieve the overall goal of suppressing system disturbances.

There are many control strategies that can be used with the active damper. Some examples are direct acceleration feedback (DAF), direct velocity feedback (DVF) and direct positional feedback (DPF). The DVF method is chosen because it does not need a model of the structure in order to synthesize a controller. Additionally, previous experiments by Mancisidor et al [13] have shown that DVF is an effective and simple control law to use for vibration damping applications using an external actuator.

4.3.1 Filters

The control law structure is defined in this section. The gain is a constant value determines the signal amplification and how much damping force the actuator induces. The gain needs to be tuned carefully due to the possibility of an unstable closed-loop system for large values of gain. In addition to the gain, other filters can be added to the direct velocity feedback controller, K as seen in Eqn. (4.1). They are used in order to shape the closed-loop frequency response. The filters are a high, low pass filter and a compensation filter.

$$K(s) = \underbrace{K_d}_{\text{Gain}} \cdot \underbrace{K_{HPF}}_{\text{High Pass Filter}} \cdot \underbrace{K_{LPF}}_{\text{Low Pass Filter}} \cdot \underbrace{K_{comp}}_{\text{Compensation}} \tag{4.1}$$

$$K_{HPF}(s) = \frac{s^2}{s^2 + 2\zeta_{HPF}\omega_{HPF}s + {\omega_{HPF}}^2} \tag{4.2}$$

$$K_{LPF}(s) = \frac{{\omega_{LPF}}^2}{s^2 + 2\zeta_{LPF}\omega_{LPF}s + {\omega_{LPF}}^2} \tag{4.3}$$

$$K_{comp}(s) = \frac{s^2 + 2\zeta_a\omega_a s + {\omega_a}^2}{s^2 + 2\zeta_b\omega_b s + {\omega_b}^2} \tag{4.4}$$

The high and low pass filters are second order and its structure can be seen in Eqn. (4.2) and Eqn. (4.3), respectively. The natural frequency (ω) specifies the filtering frequency and the damping ratio (ζ) determines the amplitude of the filter response. The damping ratio is set to 0.707 for a critically damped response. The high pass filter protects the actuator from any low frequency noise and accelerometer drift. The low pass filter rejects high frequency noise and minimizes its effects on higher frequency modes.

The compensation filter, as seen in Eqn. (4.4), prevents the actuator from hitting its saturation limit. Usually inertial actuators contains one resonance frequency. The filter avoids the actuator resonance by changing the poles of the actuator saturation frequency to lower frequencies in which the actuator will not be affected. The terms ω_a and ζ_a represent the natural frequency and damping ratio of the actuator. The terms ω_b and ζ_b represent the natural frequency and damping ratio where the actuator dynamics will be shifted to.

4.4 Frequency Based Autotuning

The need for autotuning arises when the configuration of the machine tool structure and the cutting conditions change. An example of this can be seen in Figure 4-3 where the structural modes change in

amplitude and frequency with the varying length of the ram overhang in the machine tool structure. The depth of cut is minimized as the ram overhang extends and the amplitude of the vibration mode is increased. The ram behaves like a cantilever beam and its flexibility increases as it extends outwards. The controller tuning becomes a tedious task if a controller needs to be manually tuned for all of the different machining configurations on each individual machine. Thus, an automatic method of tuning the controller parameters is needed to find the optimal parameter values as well as reduce the engineering time required to tune the controller.

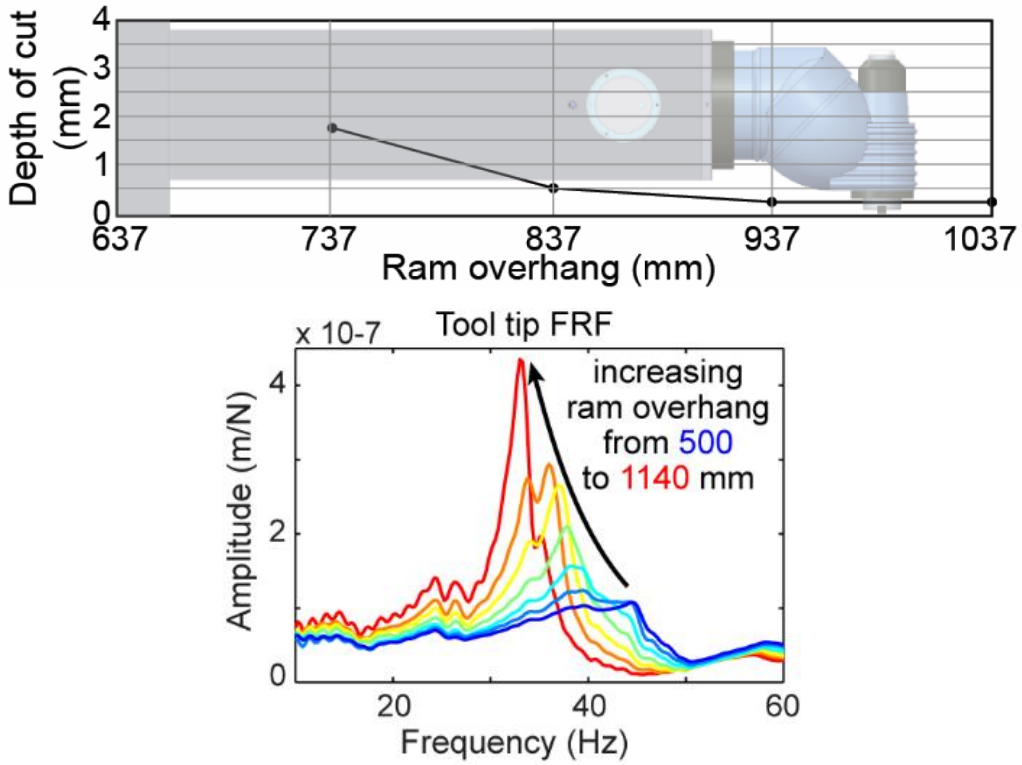

Figure 4-3 FRF of machine with varying ram overhang length [3]

4.4.1 Closed-loop Response Prediction

Optimal closed-loop FRFs for each machine location and ram overhang are generated in simulation and then experimentally verified. Time is saved by evaluating the controller performances in simulation rather than experimentally verifying each differing controller on the machine tool. The effects of the controller on the closed-loop response of the system can be predicted by the research done by Xavier et al [3]. The equations required can be seen in Eqn. (4.5) and Eqn. (4.6). The control loop from which the equations

are derived from is seen in Figure 4-4. Two FRFs need to be collected in order to generate the prediction model: one open-loop FRF and one closed-loop FRF conducted with a simple initial controller.

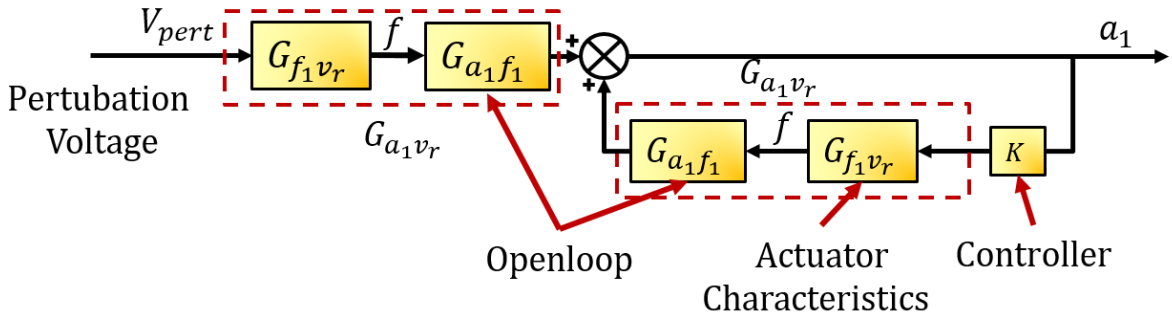

Figure 4-4 Active damping control loop structure

$$\underbrace{G_{a_1f_1}^{clp}}_{\text{Closed-loop Response}} = \underbrace{\frac{1}{1+G_{a_1v_r}K}}_{\text{Modifying Term}} \times \underbrace{G_{a_1f_1}}_{\text{Open loop Response}} \tag{4.5}$$

K	Controller
$G_{a_1f_1}$	Closed-loop FRF
$G_{a_1f_1}^{clp}$	Control to Actuator Output
$G_{a_1v_r}$	Open-loop FRF

$$G_{a_1v_r} = \frac{G_{a_1f_1} - G_{a_1f_1}^{clp0}}{K^0 \cdot G_{a_1f_1}^{clp0}} \tag{4.6}$$

K^0	Initial Controller
$G_{a_1f_1}^{clp0}$	Initial Closed-loop FRF

With this prediction model, the feedback controller can be designed virtually in a simulation and its effect on the closed-loop response of the system can be predicted.

4.4.2 Objective Function

With the prediction tool and the structure of the DVF controller set, the optimal controller can then be calculated. First, a range of acceptable controller parameter values is defined for the auto-tuning procedure. The effects of each set of controller parameter value on the closed-loop response are then evaluated based on an objective function. The best controller parameter that maximizes the damping of the system vibration modes while meeting performance constraints and system stability is then selected to be used. The area underneath the magnitude of the FRF is used as the objective function. As the objective function is minimized, the vibration modes will be minimized as well.

4.4.3 Stability Check

The stability of the closed-loop response is determined by applying the Nyquist stability criterion on the predicted closed-loop response [29]. Constraints are defined to help shape the closed-loop frequency response function. The constraints that can be set are the frequency range of interest, max sensitivity and co-sensitivity amplitudes, max controller gain and max amplitude of the magnitude FRF. The constraints will direct the procedure on the region it needs to minimize, to avoid actuator saturation and what system performance it needs to aim for in terms of sensitivity and co-sensitivity.

The auto-tuning procedure can be seen in Figure 4-5. First, user defined ranges of controller variable values are iterated through simulation. The predicted closed-loop response is then evaluated on its performance and stability. The objective function value is defined as the area underneath the FRF curve. The objective function will maximize system performance and prevents instabilities from being introduced into the system. The controller with the best objective function value is then selected.

4.5 Experimental Validation

Experimental validation of the auto-tuning method has been carried out by conducting different case studies to validate the simulated responses on different machines, machine configurations and with different damping actuators. Two different machining setups are used for the experimentation. A FMT machining center from Soraluce with a Dynamics Active Stabilizer (DAS) system equipped and a workpiece to be machined mounted with a portable damper. A DAS system is the name for the embedded actuator found within the Soraluce milling machines. Figures of the FMT and portable damper setup is seen in Figure 4-6 and Figure 4-8, respectively.

4.5.1 Experimental Setup

The vibration modes within the system will appear in the measured FRF. Accelerometers will be used to capture the raw acceleration data and the subsequent calculated FRF will display the vibration modes. In the FMT system with the DAS, there are accelerometers embedded within the ram of the machine. In the portable damper system, an accelerometer is mounted on the opposite face of the thin-walled workpiece. Open loop and closed-loop responses are obtained via a sinestream sweep signal.

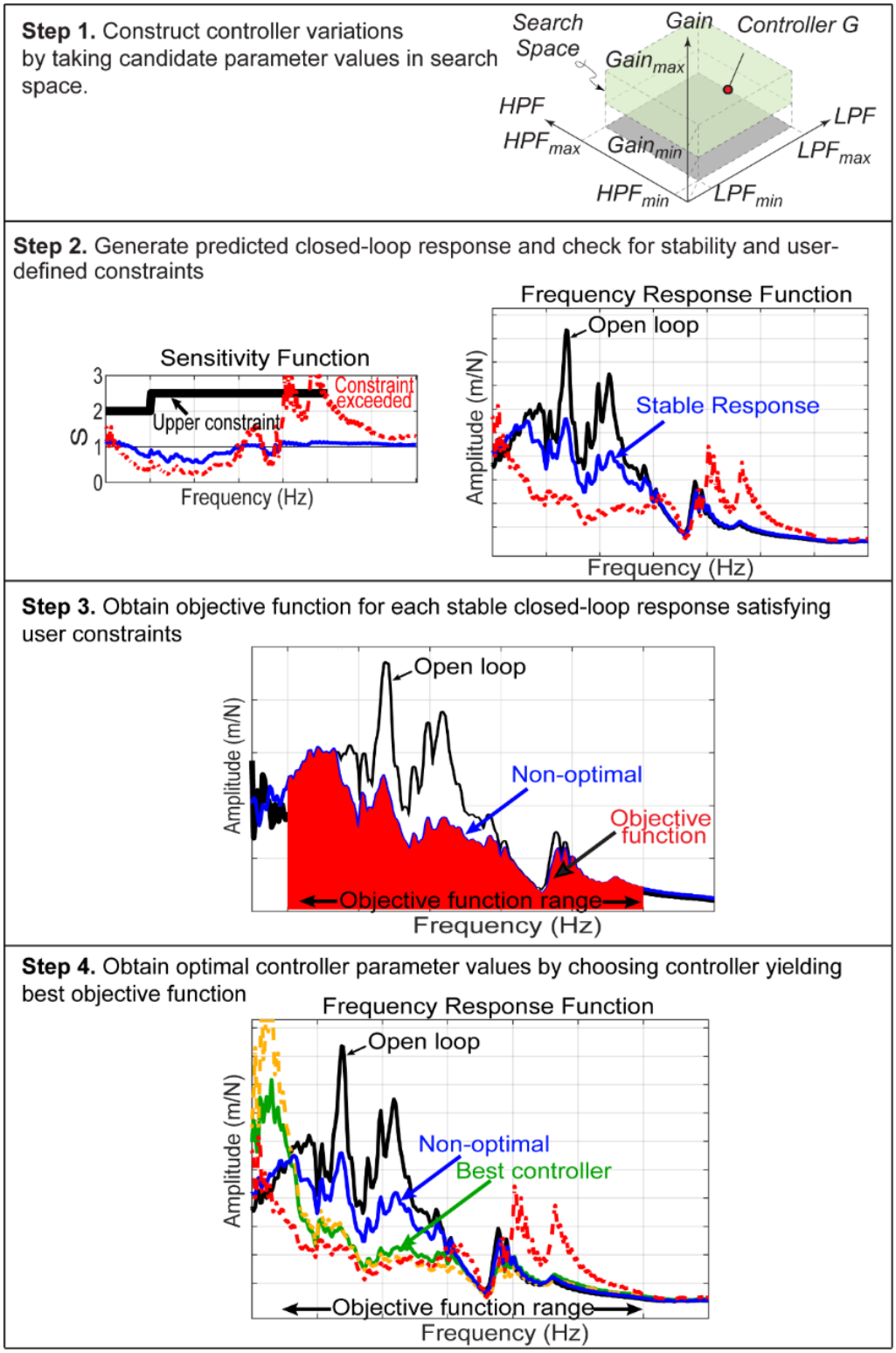

Figure 4-5 Procedure for autotuning DVF controller

4.5.2 Soraluce Milling Center

The auto-tuning procedure has been successfully implemented on a machine tool structure from Soraluce. The auto-tuned controller can be seen in Figure 4-7 in green. The manually tuned controller is shown in the comparison as the blue non-optimal controller. It can be seen that the optimal controller has a better performance in damping the vibration modes within the desired frequency rangemojntied . The controller was designed in under 30 seconds using the auto-tuning method whereas the manually tuned controller requires numerous trial and error cycles and needs an experienced controls engineer who understands the system to tune the controller.

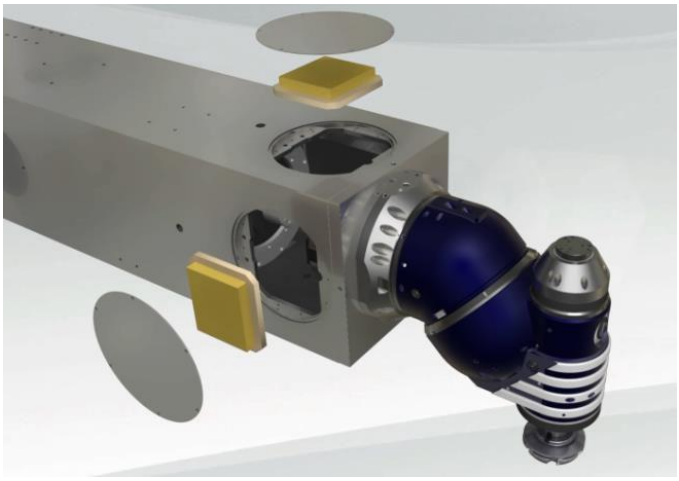

Figure 4-6 Soraluce FMT machining center with DAS system

The sensitivity function of the closed-loop response was constrained during the tuning of the controller as seen in the Figure 4-7. Closed-loop responses from other controller trials can be seen in the figure as well. Controllers that result in responses exceeding the constraints or give an unstable system response are discarded.

The auto-tuning method has been tested on various portable dampers on different structures at IK4-Ideko and on DAS systems on Soraluce milling machines with success. Currently the auto-tuning procedure is in the final testing stages before the feature is implemented on the Soraluce milling machines and with portable damping systems on individual workpieces.

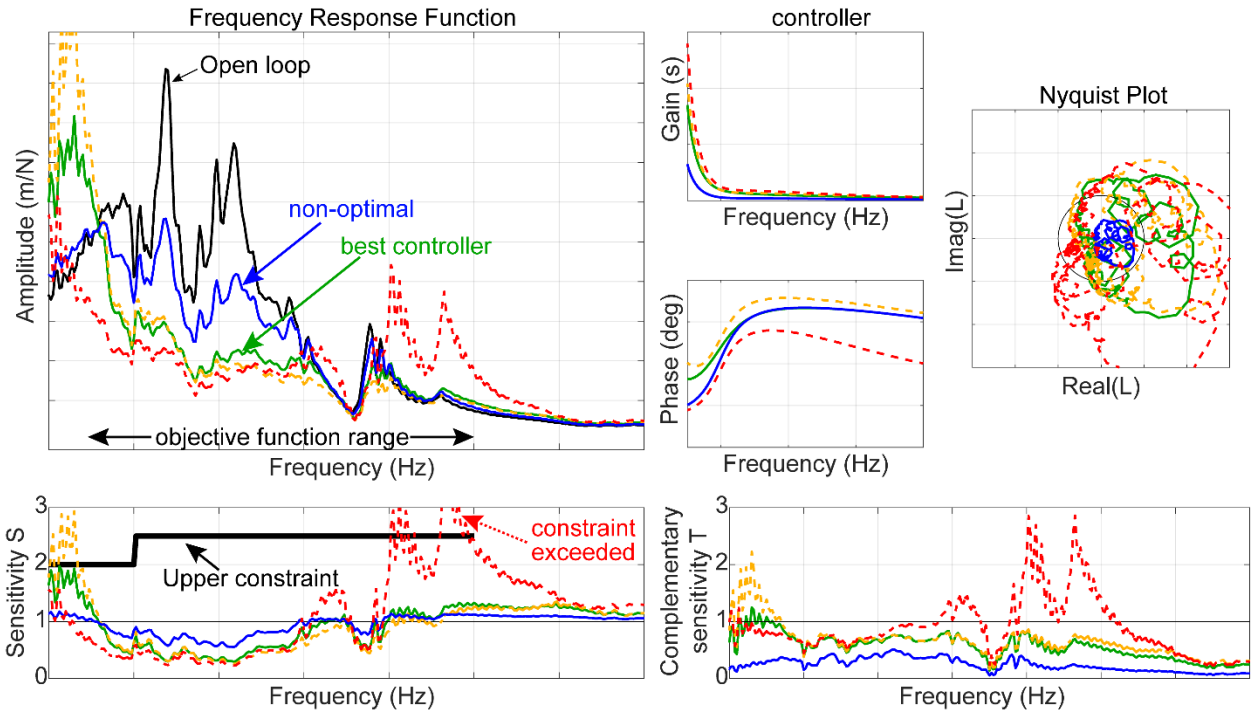

Figure 4-7 Soraluce machine autotuned closed-loop results

4.5.3 Box Shaped Workpiece

Active damping of a box shaped workpiece has also been tested. The box is constructed by welding thin plates of steel together. When one of the faces of the box is machined as part of a post processing process, chatter vibrations can appear due to the vibrations of the thinness of the side faces. When an actuator is mounted to the opposite face of the workpiece, it adds additional damping to the face and minimize the chatter vibrations. The result is a better surface finish and less forces induced on the cutter.

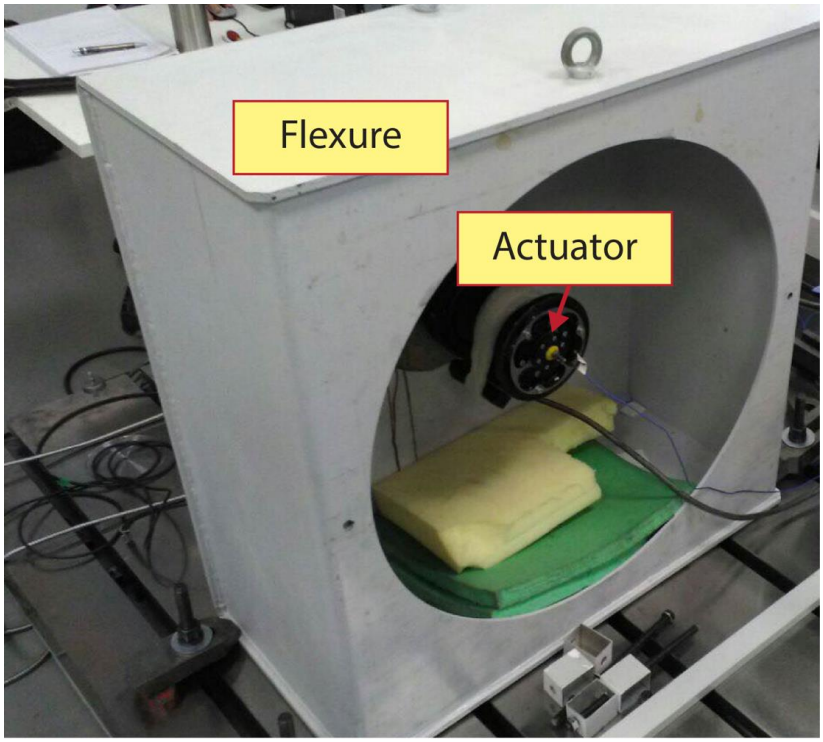

Figure 4-8 Portable damper mounted on workpiece

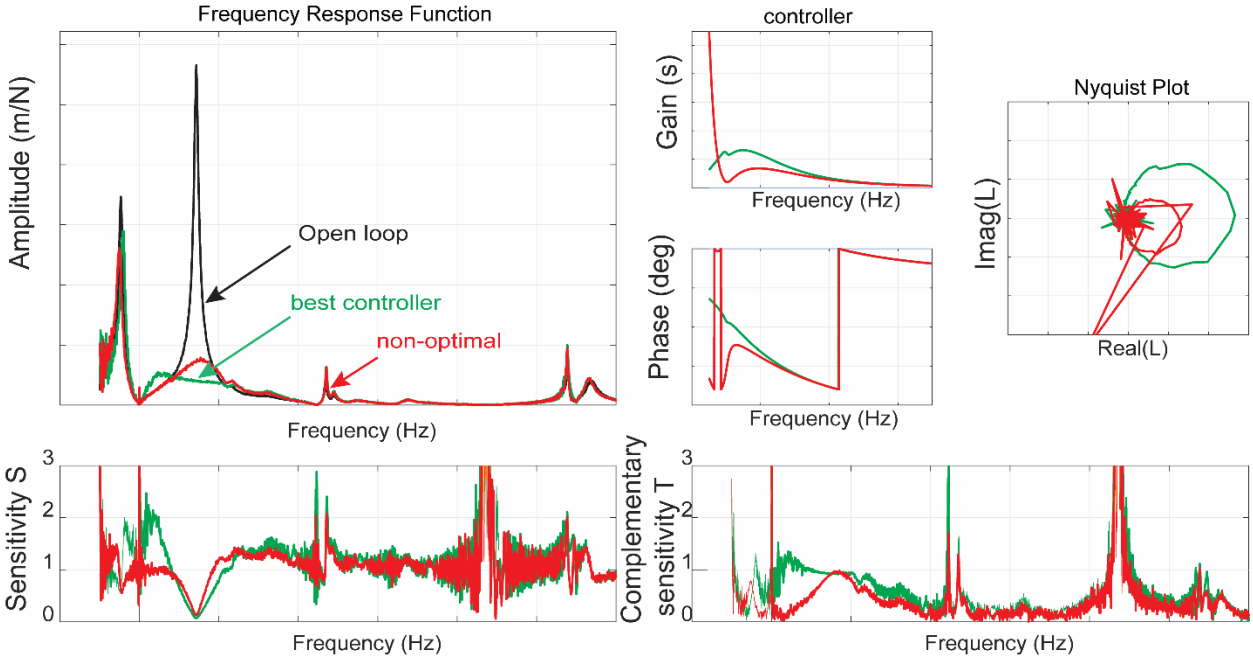

Figure 4-9 Workpiece autotuned closed-loop results

4.6 Drawbacks

There are a few instances where the auto-tuning procedure does not improve the damping of the structural modes. For instance, this occurs in the case of counter-phase modes where some modes are damped but others are destabilized. This has been observed in non-collocated systems where the sensing and actuating point are in different locations. For example, this happens when the column of the machine tool is turning in one direction and the ram is bending in the other direction as seen in Figure 4-10.

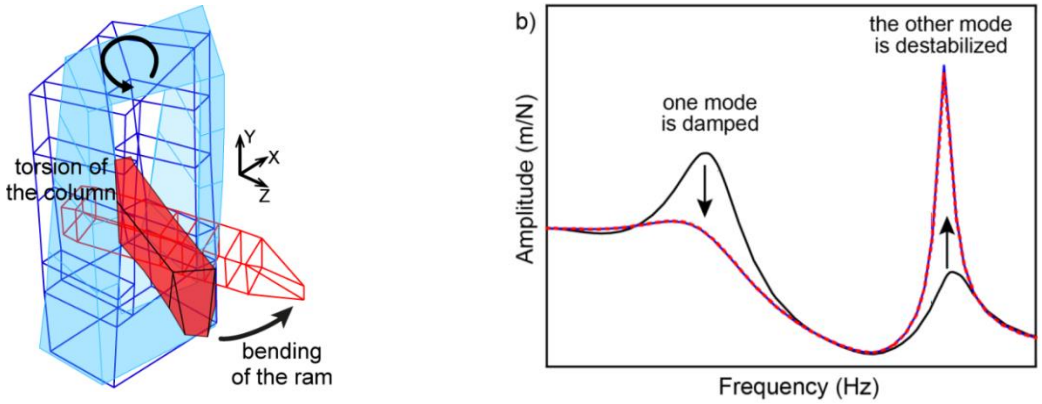

Figure 4-10 Counter-phase mode behavior [25]

4.7 Conclusion

In this chapter, an automated method of tuning controller values is presented. A model for predicting closed-loop response from different feedback controllers in simulation is used. The prediction model allows different controllers to be tested in simulation and an optimal controller to be found by iterating through controller parameter values and choosing the controller with the best objective function. User defined constraints and stability checks are used to ensure closed-loop stability and good performance. The auto-tuning method has been experimentally verified on a Soraluce milling center and on portable dampers acting on workpieces by obtaining closed-loop FRFs and comparing the optimal controllers found against manually tuned controllers. The correlation between the simulation and experimental results of optimal controllers are very good. The small discrepancies can be due to the inaccuracies in the prediction model. One solution is to obtain several FRFs when generating the prediction model so that the model is built on an average and the averaged model can filter out the inaccuracies. One issue that the auto-tuning method does not address is the case when there are counter-phase modes in the system. In Chapter 5 and Chapter 6 a model-based controller technique will be presented to solve the issue of counter-phase modes.

Chapter 5
Frequency Domain Curve Fitting Algorithm

5.1 Introduction

Curve-fitting algorithms are used to create a mathematical model that estimates the system's parameters from the measured FRFs. This process is referred to as modal parameter extraction [26]. This allows engineers and researchers to analyze the system parameters such as natural frequency and damping ratio to verify design simulations and evaluate system performance. In this chapter, a new automatic frequency domain based curve-fitting algorithm is introduced. This algorithm is used to identify modal parameters within mechanical structural systems. The model will then be used later on in Chapter 6 in the generation of model-based controllers that are able damp complex structural vibration modes.

A brief background explanation in vibration mode modeling is explained in Section 5.2. The curve fitting algorithm is explained in Section 5.3. Experimental results and comparisons are presented in Section 5.4, followed by conclusions in Section 5.5.

5.2 Vibration Mode Model

A simplified model of a multi-degree of freedom (MDOF) mechanical system can be seen in Eqn. (5.1). It is a summation of 2nd order equations in which each equation represents a vibration mode with its own natural frequency (ω_k), damping ratio (ζ_k) and modal constant or residue (α, β). This is the model that will be used to fit the measured FRFs of mechanical systems.

$$G = \sum_{k=1}^{N} \frac{\beta_k s + \alpha_k}{s^2 + 2\zeta_k \omega_k s + {\omega_k}^2} \tag{5.1}$$

5.3 Automatic Curve Fitting

The general steps for conducting the curve fitting of the FRF is as follows:

1. Calculate initial estimates of natural frequency and damping ratio for selected modes
2. Obtain initial modeled response and calculate difference between measured and modeled
3. Fit remaining dynamics and readjust previously calculated model parameters
4. If necessary, use optimization to improve global optimality

Detailed explanations of the steps are presented in the following sections.

5.3.1 Initial Estimate of Damping and Natural Frequency of a Mode

The user first selects the vibration modes that are required for fitting by looking at the magnitude FRF. The highest peaks in the FRF represent the system vibration modes. An example can be seen in Fig. Figure 5-1.

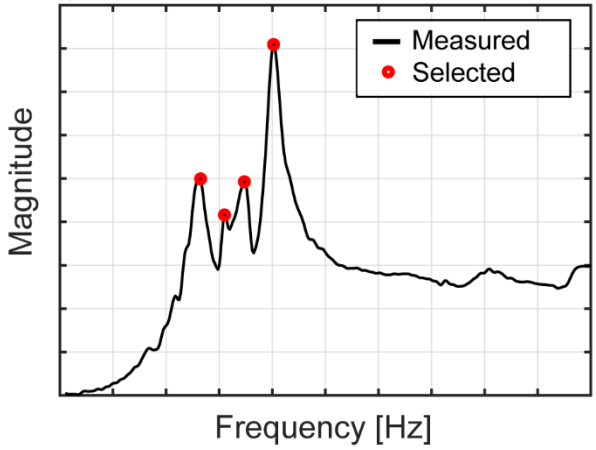

Figure 5-1 User selected modes to fit

The 2nd order equation for a vibration mode in frequency domain can be reformulated as seen by Eqn. (5.2). The residual term represents the effects of other modes outside of the measured range on the measured FRF.

$$G_k(\omega) = \underbrace{r_k + jq_k}_{Residual\ Term} + \underbrace{\frac{j\beta_k\omega + \alpha_k}{\rho - \omega^2 + j\omega\sigma}}_{Mode\ Being\ Fitted} \qquad (5.2)$$

$$\sigma = 2\zeta_k\omega_k \qquad \omega_k = \sqrt{\rho}$$

The natural frequency and damping ratio for each vibration mode in the experimental FRF are identified via least squares (LS) estimation. The regressor matrix (Φ) can be constructed by selecting the real (g) and imaginary (h) components of the experimental FRF in the frequency range of the mode being fitted. Firstly, some formulations are defined to setup the LS problem. The overall measured FRF can be represented by its real and imaginary parts as seen in Eqn. (5.3).

$$G_m = g + jh \tag{5.3}$$

The error E between fittings can be defined as the difference between measured FRF in the frequency range of the vibration mode and the vibration mode model.

$$\begin{aligned} E &\cong G_m - G \\ &\cong g_k + jh_k - r_k - jq_k - \frac{j\beta_k\omega + \alpha_k}{\rho - \omega^2 + j\omega\sigma} \end{aligned} \tag{5.4}$$

The assumption that error between the measured FRF and the model is zero is made. This is to create a relationship between the measured data and the unsolved model variables. With the assumption made, the combined formulation can be separated into real and imaginary components as seen in Eqn. (5.6) and (5.7).

$$\begin{aligned} E &= 0 \\ &= \Big((g_k - r_k) + j(h_k - q_k)\Big)(\rho - \omega^2 + j\omega\sigma) - j\beta_k\omega - \alpha_k \end{aligned} \tag{5.5}$$

Real: (5.6)

$$g\,\rho - \omega^2 g_k - r_k\rho + \omega^2 r - \omega h_k\sigma + \omega q_k\sigma - \alpha_k = 0$$

Imaginary: (5.7)

$$h\,\rho - \omega^2 h_k - q_k\rho + \omega^2 q - \omega g_k\sigma + \omega r_k\sigma - \omega\beta_k = 0$$

With the real and imaginary parts defined, the LS problem structure can be constructed and solved using the real and imaginary parts as follows:

$$\begin{aligned} Y &= \Phi\theta \\ Y &= [g_k \quad h_k]^T \\ \theta^T &= [\rho \quad r_k\rho \quad q_k\rho \quad \sigma \quad r_k\sigma \quad q_k\sigma \quad r_k \quad q_k \quad \alpha_k \quad \beta_k] \\ \Phi &= \begin{bmatrix} \omega^{-2}g_k & -\omega^{-2} & 0 & -\omega^{-1}h_k & 0 & \omega^{-1} & 1 & 0 & -\omega^{-2} & 0 \\ \omega^{-2}h_k & 0 & -\omega^{-2} & \omega^{-1}g_k & -\omega^{-1} & 0 & 0 & 1 & 0 & -\omega^{-1} \end{bmatrix} \end{aligned} \tag{5.8}$$

$$\omega_k = \sqrt{\rho} \qquad \zeta_k = \frac{\sigma}{2\omega_k} \tag{5.9}$$

The frequency range (ω) of each vibration mode needs to be calculated in order to solve the LS problem. This can be determined by inspecting the mobility (i.e., velocity response to force) Nyquist plot for the selected mode. For linear mechanical systems with viscous damping, the mobility plot forms an exact

circle [4]. The frequency range is selected at points on the mobility Nyquist plot. First, a fixed number of experimental data points (typically at least 6) around the frequency of the user-selected mode is taken to create a circle via LS **[26]**. This circle would represent the mobility Nyquist circle for that mode. Afterwards, starting from the start and end of the 6 points, the lower and upper frequency range values for the mode are extended until values fall outside a specified boundary of the mobility circle. This means the values are no longer contributing to the current vibration mode. The procedure can be seen in Figure 5-2. Figure 5-3 displays the frequency range of all the selected modes to fit.

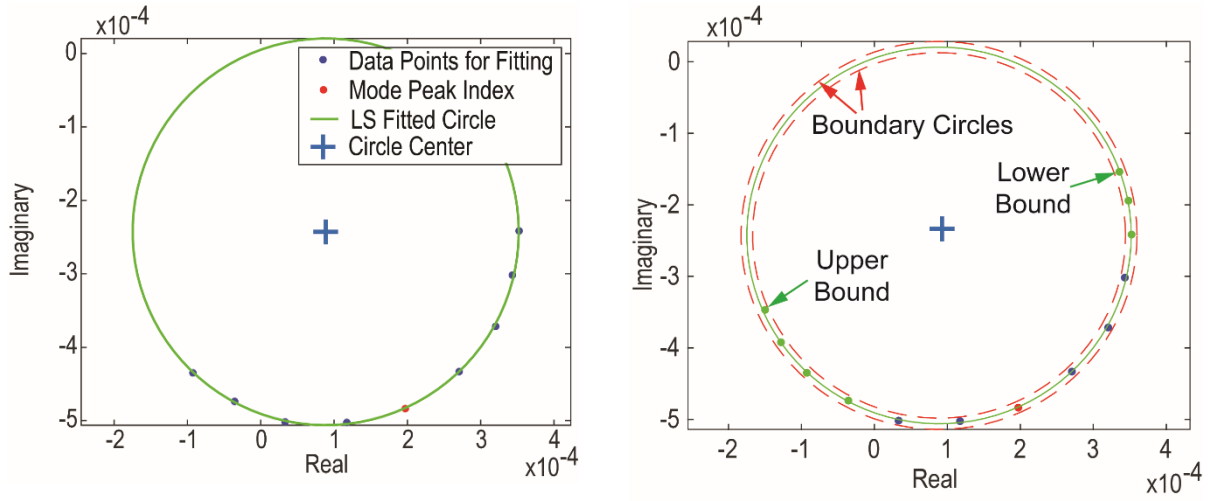

Figure 5-2 Frequency range selection from mobility Nyquist circle

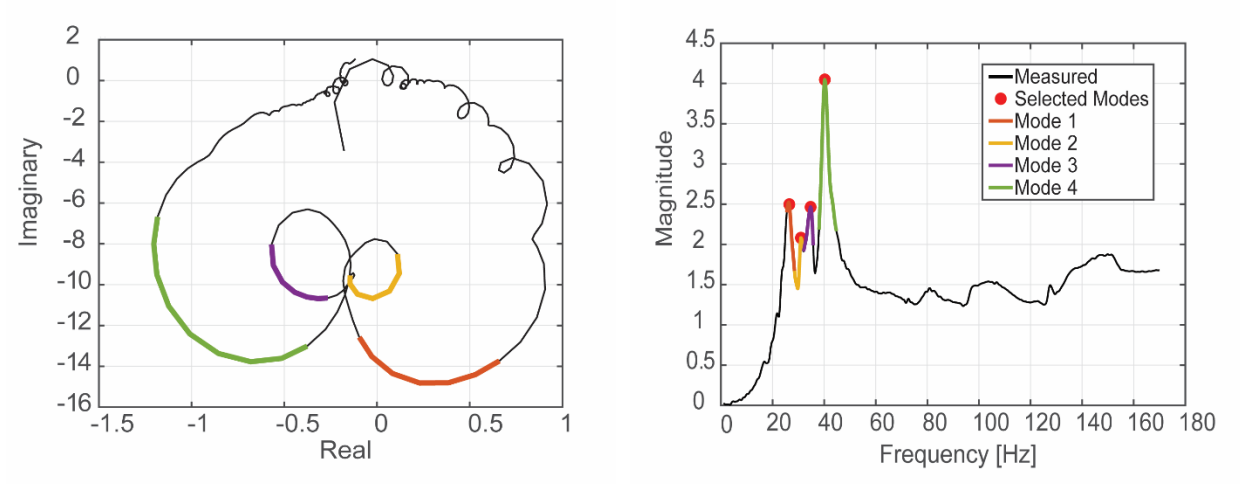

Figure 5-3 Frequency range search for mode fitting

5.3.2 Estimation of Residues and Residual Terms

After the natural frequency (ω_n) and damping ratio (ζ) terms for each mode have been identified by solving the least squares problem in Section 5.3.1, the terms of the residue (α, β) and the residual terms (a, b, c, d) can be estimated by defining a LS problem between the measured FRF data and the identified ω_n and ζ parameters. The residual terms come from the modes that exist but are not analyzed. The most common residual terms come from modes outside of the frequency range for curve-fitting.

$$G_k = \frac{a_k}{s^2} + \frac{b_k}{s} + c_k + d_k s + \frac{\beta_k s + \alpha_k}{s^2 + 2\zeta_k \omega_k s + {\omega_k}^2} \tag{5.10}$$

The measured FRF in Eqn. (5.3) can be equated to the model in Eqn. (5.10). First, a small transformation is performed on the denominator of the 2nd order term of Eqn. (5.10) for easier calculation.

$$\begin{aligned} G_d &= \frac{1}{s^2 + 2\zeta_k \omega_k s + {\omega_k}^2} \\ &= \frac{1}{{\omega_k}^2 - \omega^2 + j2\zeta_k \omega_k \omega} \\ &= \frac{1}{{\omega_k}^2 - \omega^2 + j2\zeta_k \omega_k \omega} \cdot \frac{{\omega_k}^2 - \omega^2 - j2\zeta_k \omega_k \omega}{{\omega_k}^2 - \omega^2 - j2\zeta_k \omega_k \omega} \\ &= \frac{{\omega_k}^2 - \omega^2}{({\omega_k}^2 - \omega^2)^2 + \left(2\zeta_k \omega_k \omega\right)^2} + j \cdot \frac{-2\zeta_k \omega_k \omega}{({\omega_k}^2 - \omega^2)^2 + \left(2\zeta_k \omega_k \omega\right)^2} \\ &= g_d + j h_d \end{aligned} \tag{5.11}$$

After the transformation is performed, the real and imaginary parts can now be separated along with the known and unknown variables. The measured FRF data in the frequency range of an individual vibration mode to be fitted is equated to the vibration mode model.

$$\begin{aligned} G_m &= g + jh = G_k \\ &= \frac{a_k}{s^2} + \frac{b_k}{s} + c_k + d_k s + \frac{\beta_k s + \alpha_k}{s^2 + 2\zeta_k \omega_k s + {\omega_k}^2} \\ &= \left(\frac{-a_k}{\omega^2}\right) + \left(\frac{-jb_k}{\omega^2}\right) + c_k + d_k \cdot j\omega + \alpha_k \cdot (g_d + jh_d) + \beta_k \cdot j\omega \cdot (g_d + jh_d) \end{aligned} \tag{5.12}$$

Real:

$$g = \left(\frac{-a_k}{\omega^2}\right) + c_k + \alpha_k \cdot g_d + \beta_k \cdot (-\omega h_d)$$

Imaginary:

$$h = \left(\frac{-b_k}{\omega}\right) + d_k \cdot \omega + \alpha_k \cdot h_d + \beta_k \cdot (\omega g_d)$$

With the real and imaginary components now separated into the known and unknown variables, a LS problem can now be constructed.

$$Y = \Phi\theta$$

$$Y = [g \quad h]^T$$

$$\theta^T = [a \quad b \quad c \quad d \quad \alpha \quad \beta] \tag{5.13}$$

$$\Phi = \begin{bmatrix} \Phi_{real} \\ \Phi_{imag} \end{bmatrix} = \begin{bmatrix} \omega^{-2} & 0 & 1 & 0 & g_d & -\omega h_d \\ 0 & \omega^{-1} & 0 & \omega & h_d & \omega g_d \end{bmatrix}$$

By solving the LS problem the modal participation factors and the residue terms are found. The model can now generate an initial estimated response. The initial model fitting results can be seen in Figure 5-4.

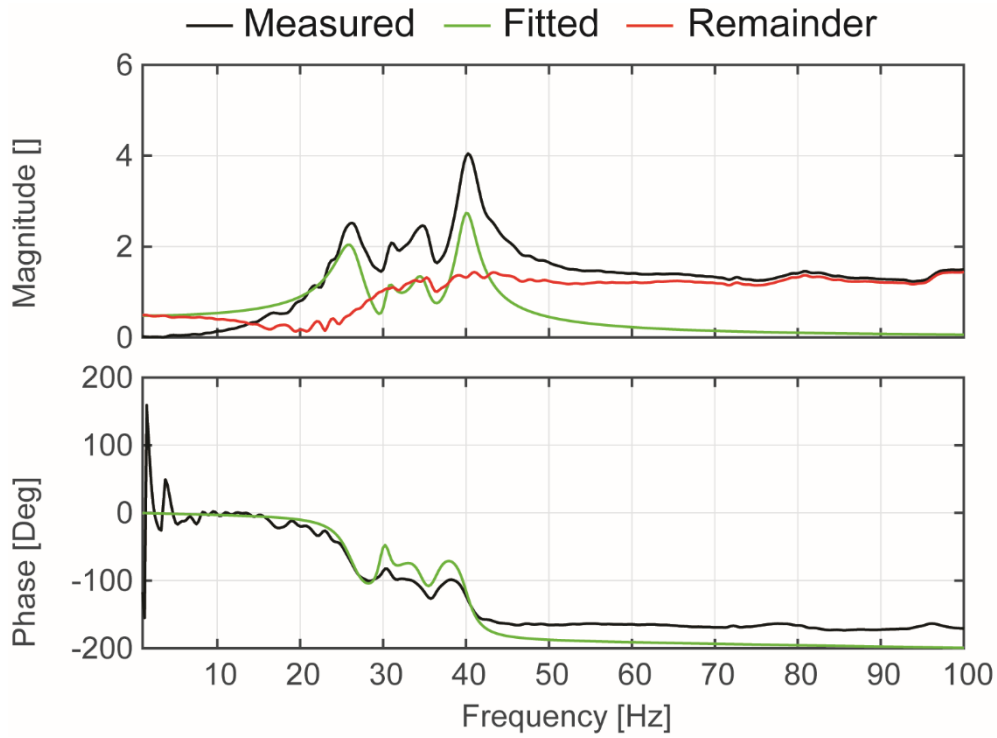

Figure 5-4 Initial FRF fitting results

5.3.3 Estimation of Reminder Dynamics

As seen above, there are additional dynamics observed within the system that are not represented by the vibration modes. This can be calculated by subtracting the fitted model FRF from the measured FRF. By modeling the remainder dynamics terms and adding them to the model, the overall fit of the FRF can be improved. The remainder dynamics are approximated by a rational fractional polynomial, as seen in Eqn. (5.14). A MATLAB function called *tfest* is used to estimate the remaining dynamics in the rational fractional polynomial form [30]. The modeled remainder dynamics are then added to the overall model and used to adjust the residual terms and residues to improve global fit.

$$G_{remainder} = \frac{b_m s^m + b_1 s^{m-1} + \cdots + b_0}{s^m + a_{m-1} s^m + \cdots + a_0} \tag{5.14}$$

5.3.4 Global Improvement of Residues and Residual Terms

At this stage, the model poles have been identified along with the remaining dynamics. By using the fitted remainder dynamics model, the global fit of the model FRF can now be improved upon. The residue terms of the vibration modes can be recalculated with the effects of remainder dynamics accounted for in a LS problem.

$$G_m + E = \sum_{k=1}^{N} G_k + G_{remainder} \tag{5.15}$$

Firstly, the reformulation from Section 5.3.2 of the denominator term ($g_d + jh_d$) is used to separate the second order term transfer function of the vibration mode into real and imaginary components.

$$\begin{aligned} N(\omega) &= \frac{\beta_k s + \alpha_k}{s^2 + 2\zeta_k \omega_k s + {\omega_k}^2} \\ &= (\beta_k s + \alpha_k)(g_d + jh_k) \\ &= (\alpha_k g_d - \omega \beta_k h_k) + j(\alpha_k h + \omega \beta_k g_d) \end{aligned} \tag{5.16}$$

Next, the remainder dynamics terms are reformulated into its real and imaginary components as well. The denominator of the remainder dynamics is first reformulated for convenience.

$$
\begin{aligned}
R(\omega) &= \frac{1}{a_0 + a_1 j\omega + \cdots + a_{n-1} j^{n-1}\omega^{n-1} + j^n\omega^n} \\
&= \frac{1}{[a_0 - a_2\omega^2 + a_4\omega^4 + \cdots] + j[a_1\omega - a_3\omega^3 + a_5\omega^5 + \cdots]} \\
&= \frac{1}{t(\omega) + ju(\omega)} \cdot \frac{t(\omega) - ju(\omega)}{t(\omega) - ju(\omega)} \\
&= \frac{t(\omega)}{t^2(\omega) + u^2(\omega)} \cdot j\frac{-ju(\omega)}{t^2(\omega) + u^2(\omega)} \\
&= p(\omega) + jq(\omega)
\end{aligned}
\tag{5.17}
$$

$$
\begin{aligned}
G_{remainder} &= (b_0 + jb_1 + j^2\omega^2 b_2 + \cdots)\big(p(\omega) + jq(\omega)\big) \\
&= \big[(b_0 - \omega^2 b_2 + \omega^4 b_4 - \cdots)p + (-\omega b_1 + \omega^3 b_3 - \omega^5 b_5 + \cdots)q\big] \ldots \\
&\quad + j\big[(b_0 - \omega^2 b_2 + \omega^4 b_4 - \cdots)q + (-\omega b_1 + \omega^3 b_3 - \omega^5 b_5 + \cdots)p\big] \\
&= [p \quad -\omega q \quad -\omega^2 p \quad \omega^3 q \quad \omega^4 p \quad \ldots] \cdot [b_0 \quad b_1 \quad \ldots]^T \ldots \\
&\quad + j[q \quad -\omega p \quad -\omega^2 q \quad \omega^3 p \quad \omega^4 q \quad \ldots] \cdot [b_0 \quad b_1 \quad \ldots]^T
\end{aligned}
\tag{5.18}
$$

Now the LS problem to improve the mode residues and the remainder dynamics can be constructed and solved.

$$
\begin{aligned}
&G_m = y = \Phi \cdot \theta \\
&\theta^T = [\alpha_1 \quad \beta_1 \quad \alpha_2 \quad \beta_2 \quad \ldots \quad \alpha_N \quad \beta_N \quad b_0 \quad b_1 \quad \ldots \quad b_m] \\
&\Phi = \begin{bmatrix} \Phi_{real} \\ \Phi_{imag} \end{bmatrix} = \begin{bmatrix} g_1 & -\omega h_1 & g_2 & -\omega h_2 & \ldots & p & -\omega q & -\omega^2 p & \ldots \\ h_1 & \omega g_1 & h_2 & \omega g_2 & \ldots & q & \omega p & -\omega^2 q & \ldots \end{bmatrix}
\end{aligned}
\tag{5.19}
$$

After the LS problem is solved, the residue terms of each vibration mode and the numerator terms of the remainder dynamics have been adjusted to increase the global fit between the measured FRF and the modeled FRF. The improved FRF can be seen in Figure 5-5.

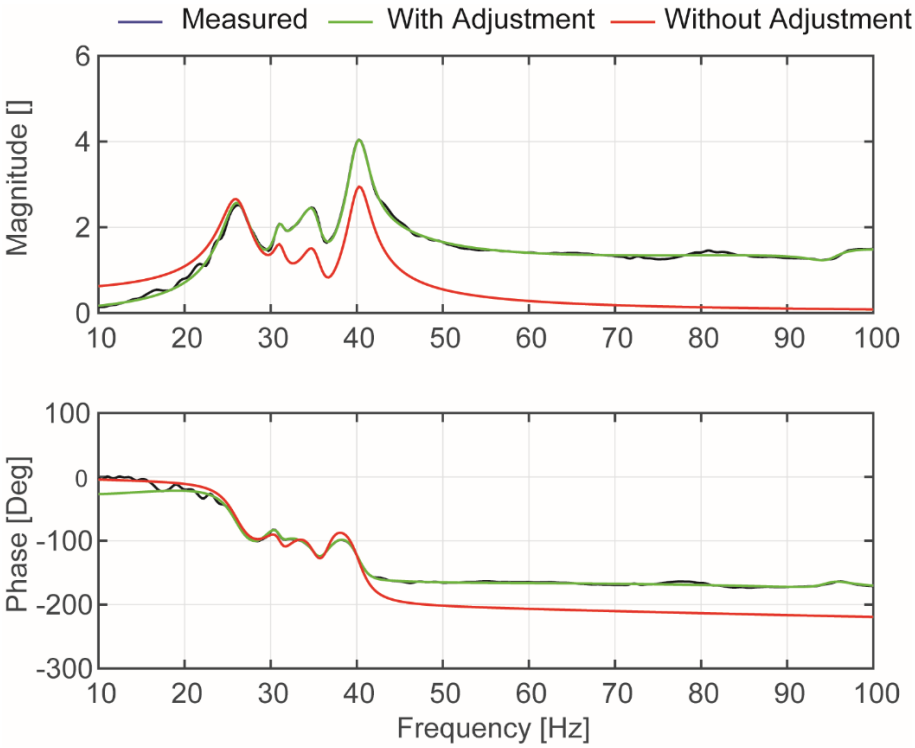

Figure 5-5 Measured and modeled FRF adjusted with remaining dynamics

5.3.5 Global Optimization

If the observed global fit was not sufficient, global search optimization can be used to improve the global fit of the FRF. A figure of the optimization steps can be seen in Figure 5-6. The real and complex conjugate pole locations (ω, ζ, p) are modulated to minimize the root mean square (RMS) error between the measured and identified FRF. The participation parameters, β_k, α_k, γ_k, and δ_k are automatically solved for each pole combination by constructing the LS sub-problem as previously introduced in section 5.3.1.

$$G(s) = \underbrace{\sum_{k=1}^{N_c} \frac{\beta_k s + \alpha_k}{s^2 + 2\zeta_k \omega_k s + \omega_k^2}}_{Complex\ Poles} + \underbrace{\sum_{k=1}^{N_r} \frac{\gamma_k}{s + p_k}}_{Real\ Poles} + \underbrace{\delta_0 + \delta_1 s + \cdots + \delta_m s^m}_{Direct\ terms} \tag{5.20}$$

Additional dynamics contributions originating from complex conjugate poles, real poles, and direct transmission-like terms can be grouped together as seen in Eqn. (5.20).

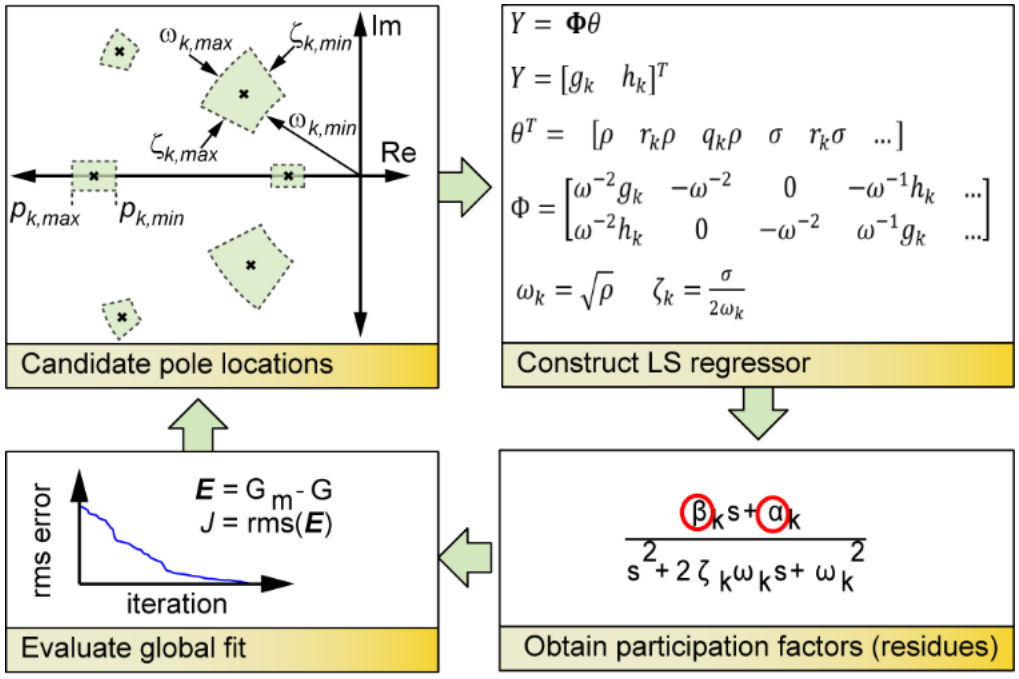

Figure 5-6 FRF model optimization steps

5.4 Experimental Results and Comparisons

The curve fitting algorithm has been tested on different workpieces at IK4-Ideko. The algorithm was compared against the MATLAB System Identification Toolbox function, *modalfit*. *Modalfit* extracts modal parameters of input FRFs. FRFs are generated by conducting frequency sweeps using portable damping actuators mounted on the workpieces. The curve fitting of two box shaped workpieces are presented in the following sections.

5.4.1 Lab Box Workpiece

A box workpiece made of welded steel sheets is clamped down on a stiff platform within the IK4-Ideko laboratory. An actuator is mounted to one face of the box. The setup can be seen in Figure 5-7. The box contains numerous vibration modes on each face due to the thin sheet metal construction. A frequency sweep was conducted from 10 to 400 Hz and the model was fitted from 10 Hz to 350 Hz. The number of modes selected to be fitted in the model is seven after viewing the measured FRF plot and selecting the modes of interest.

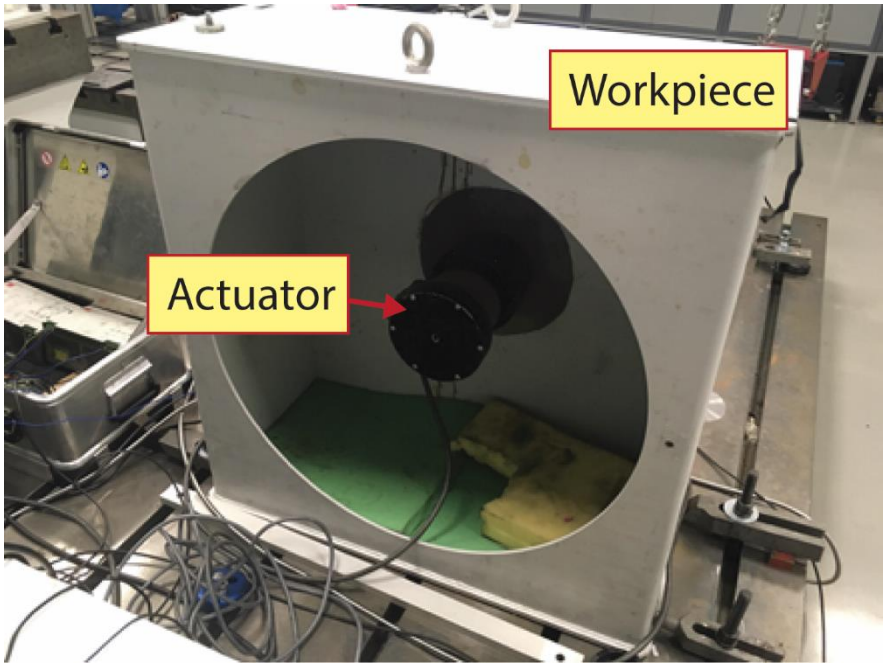

Figure 5-7 Lab box workpiece with damping actuator

The curve fitted model using the proposed method and *modalfit* can be seen in Figure 5-8. Both models are able to approximate the magnitude of the measured dynamics quite well. The derived model parameters can be seen in Table 5-2. The proposed method derived 14 vibration modes (7 selected and 7 residual vibration mode terms). The *modalfit* function derived 15 vibration modes with their respective natural frequencies and damping ratios. By observing modes of interest from the derived natural frequencies and damping ratios between the two methods, it appears that the natural frequencies and damping ratios are quite similar to from one method to another. The compared natural frequencies and damping ratios are marked by the bolded entries in Table 5-2. In terms of fit optimality, it appears that the proposed method performs better by viewing the error differences between the measured data and the fitted data in the magnitude and phase plot. It can be seen that the maximum and RMS of the magnitude and phase errors are lower using the proposed method compared to the *modalfit* function in Table 5-1.

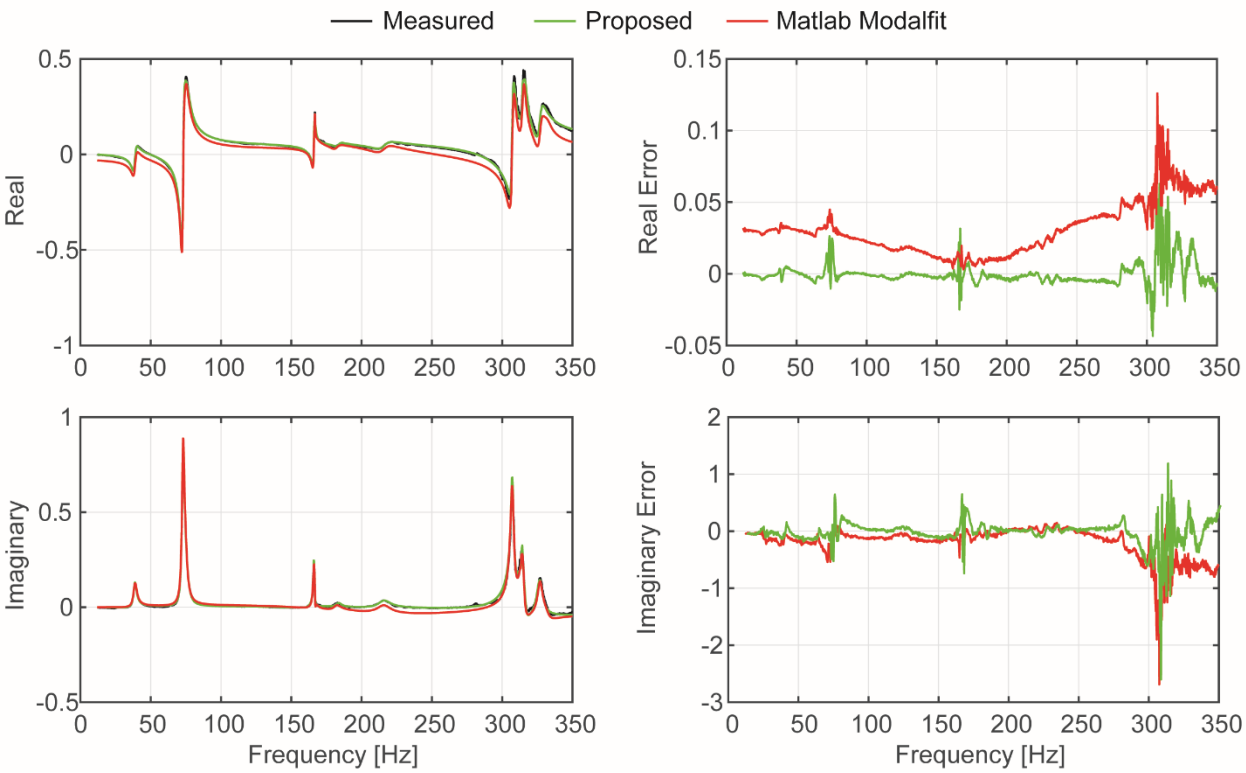

Figure 5-8 Lab workpiece model fit and error

Table 5-1 Error between data and model (lab box workpiece)

Discrepancy in curve fit	Proposed(14th Order)	MATLAB Modalfit
RMS Error	0.0125	0.0392

Table 5-2 Model parameters of lab box workpiece curve fit

Selected Modes							
Proposed					MATLAB Modalfit		
Mode	ω_n [rad/s]	ζ_n	α_k	β_k	Mode	ω_n [rad/s]	ζ_n
1	**242.35**	**0.0407**	-583.95	-0.768	1	**243.48**	**0.039**
2	**458.48**	**0.0131**	-3828.71	-1.894	2	**458.59**	**0.013**
3	**1045.33**	**0.0033**	-1405.96	1.156	3	469.05	0.021
4	**1161.82**	**0.0030**	-223.43	0.093	4	**1044.02**	**0.005**
5	**1931.43**	**0.0043**	-16818.33	3.933	5	**1048.46**	**0.002**
6	**1977.72**	**0.0044**	-8464.50	2.844	6	**1142.90**	**0.017**

7	**2053.39**	**0.0058**	-8387.32	0.678	7	1314.64	0.353
Residual Components					8	1355.17	0.027
1	4681.30	0.3028	1316515.41	12.152	9	1926.76	1.521e-05
2	2071.49	0.0053	-2960.02	0.406	10	1930.97	0.005
3	1955.09	0.0161	-11368.92	3.254	11	1968.81	4.560e-05
4	1918.55	0.0152	-1790.89	-2.443	12	1970.98	0.020
5	1365.141	0.0232	-3322.43	0.523	13	**1979.13**	**0.005**
6	1044.69	0.0146	-743.81	-1.630	14	**2054.58**	**0.006**
7	466.07	0.0285	-2780.68	1.036	15	2085.39	0.010

5.4.2 Production Box Workpiece

The curve fitting algorithm was tested on another workpiece within a production setting. The workpiece is larger in size and possess more vibration modes than the lab box workpiece. The actuator is mounted on the face of the workpiece that will undergo a surface finishing process that involves machining. The workpiece can be viewed in Figure 5-9. There are 19 modes of interest selected to be fitted in the frequency range of 30 Hz to 350 Hz. The fitting results using the proposed method and *modalfit* can be seen in Figure 5-10. The model parameters identified can be found in Table A-1. The RMS and max error can be viewed in Table 5-3. By viewing the RMS errors, it can be seen that while the proposed method models the low frequency portions well, the RMS error begins to increase at the high frequencies starting at 275 Hz. This could possibly be due to the high number of modes clustered together and the proposed method is not able to handle it well. Compared to the proposed method, *modalfit* is able to fit the measured data at high frequencies with a smaller error.

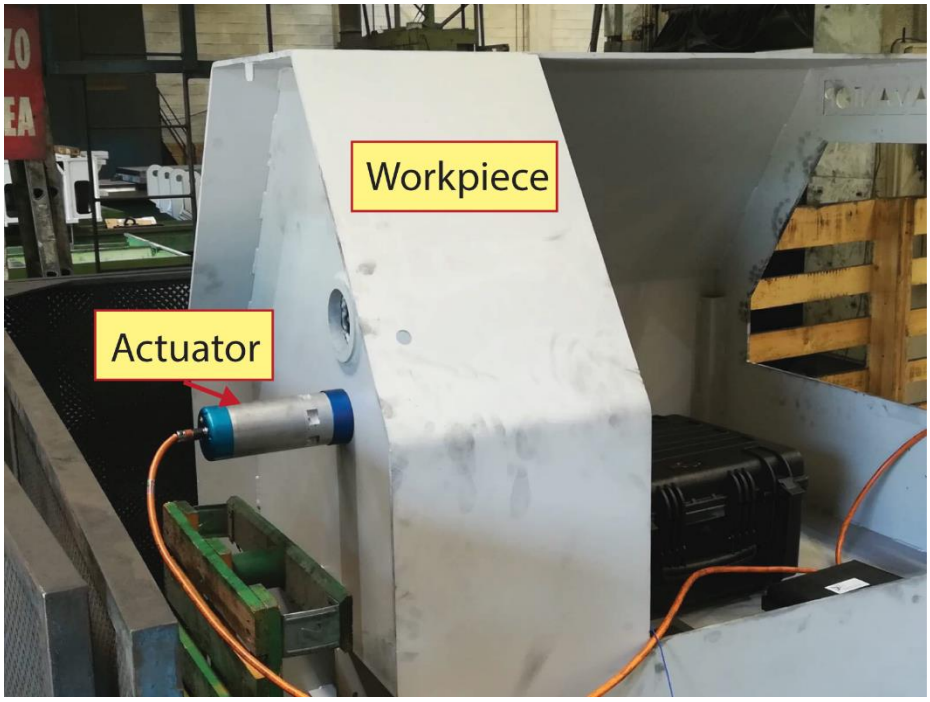

Figure 5-9 Production box workpiece with damping actuator

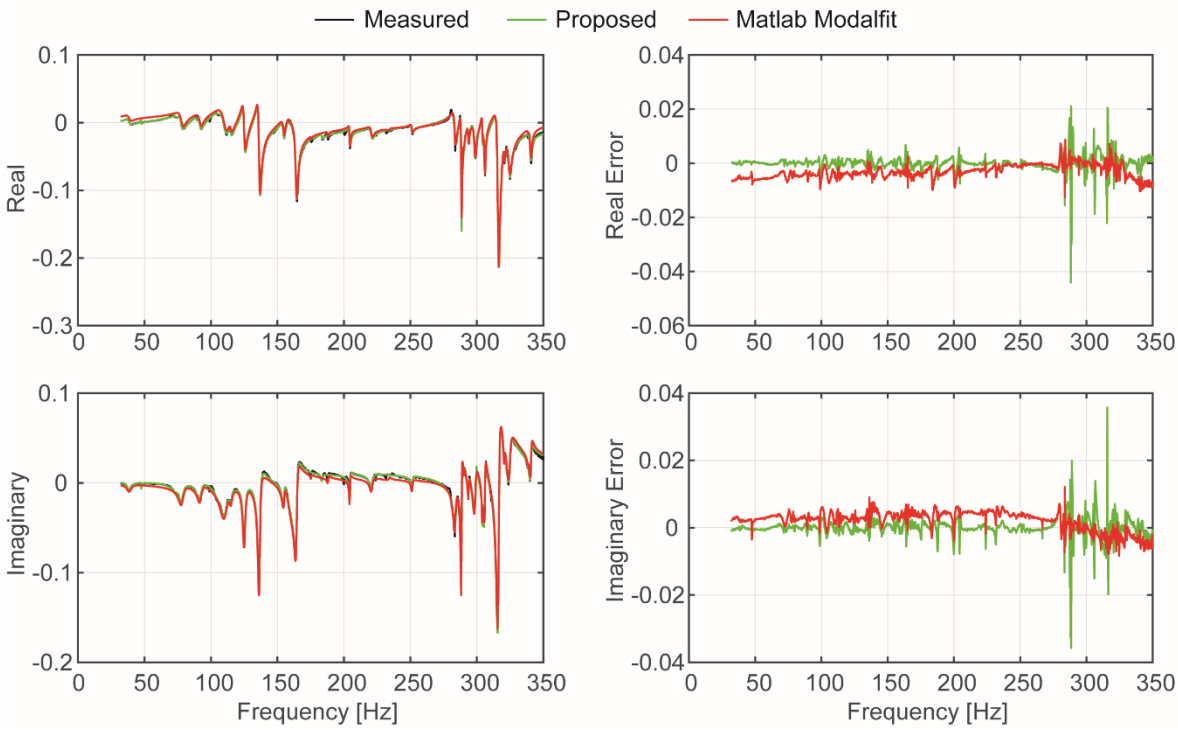

Figure 5-10 Production workpiece model fit and error

Table 5-3 Error between data and model (production box workpiece)

Discrepancy in curve fit	Proposed	MATLAB Modalfit
RMS Error:	0.0043	0.0054

5.4.3 Remarks

The proposed curve-fitting algorithm is able to determine the modal parameters of a system quite accurately as seen in the test trials. At times it is more accurate than the *modalfit* function. However, one downside of the proposed method is that the user has to manually select the vibration mode peaks to fit whereas *modalfit* does not need the peaks to be picked. Moving forward, the proposed method will be used to model the system.

5.5 Conclusion

In this chapter, an algorithm to extract modal parameters from a measured FRF was presented. Initial natural frequency and damping ratio values are found by constructing and solving a LS problem between the measured data and 2^{nd} order equation model variables. After initial fitting, the remaining dynamics that were not considered by the model are found by finding the difference between the initial fit and the measured. The remaining dynamics terms are then curve fitted and added to the overall model. With the remaining dynamics modeled, modal participation terms and remaining dynamics are then adjusted for global fit by constructing a LS problem between the measured data and the new model variables. If necessary, a global optimization step is conducted to further improve global fit. The algorithm was tested on several different workpieces and its performance compared against other fitting algorithms from within MATLAB. The new introduced algorithm performs better in structures where vibration modes are clearly defined and have separation between them.

Chapter 6
Experimental Flexure Design

6.1 Introduction

The machines that exhibit counter-phase mode behavior as seen at the end of Chapter 5 are large and costly. Thus, it is dangerous to experimentally test new control laws directly on the machines in case a controller causes instability during machine operation. A small laboratory setup has been designed in order to simulate counter-phase mode behavior in a controlled laboratory setting to experimental test out new controllers.

In this chapter, the design and validation of the experimental setup is presented. The design process is explained in Section 6.2. The experimental validation and analysis is presented in Section 6.3.

6.2 Experimental Setup Design

The experimental setup that will mimic the column and ram of a Soraluce milling machine as seen in Figure 6-2.The custom designed flexure contains two vibration modes, one in counter-phase with the other. The flexure frequency modes were designed using CAD and experimentally verified using tap testing.

6.2.1 Flexure Design

The flexure is designed to have two vibration modes, one in counter-phase with one another. The shape of the flexure is a L with two pieces of steel blocks welded together. A schematic drawing of the flexure can be seen in Figure 6-2. Plain carbon steel was selected for the two bars that comprise the L shape. Plain steel was selected because of it is easily sourced and can be welded together. The base plate that the two bars are attached to is also made of plain carbon steel. The bars and the base plate are welded together to produce a solid body.

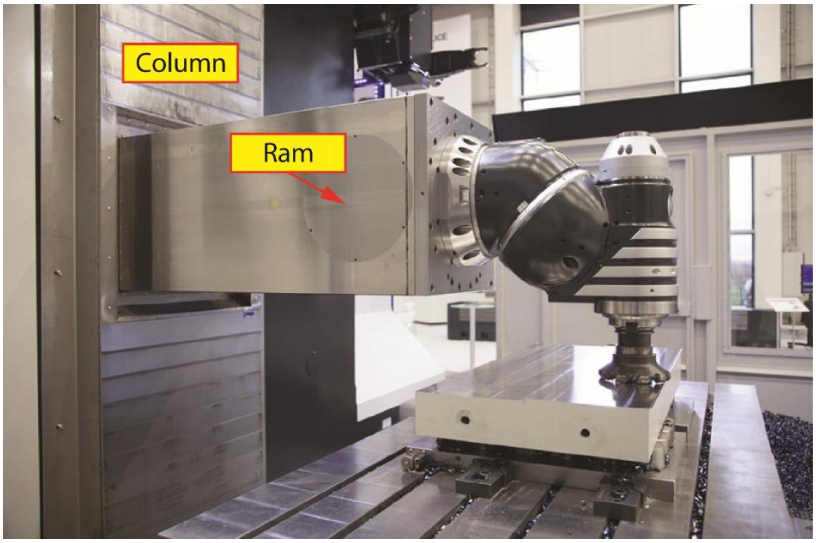

Figure 6-1 Soraluce Milling Machine

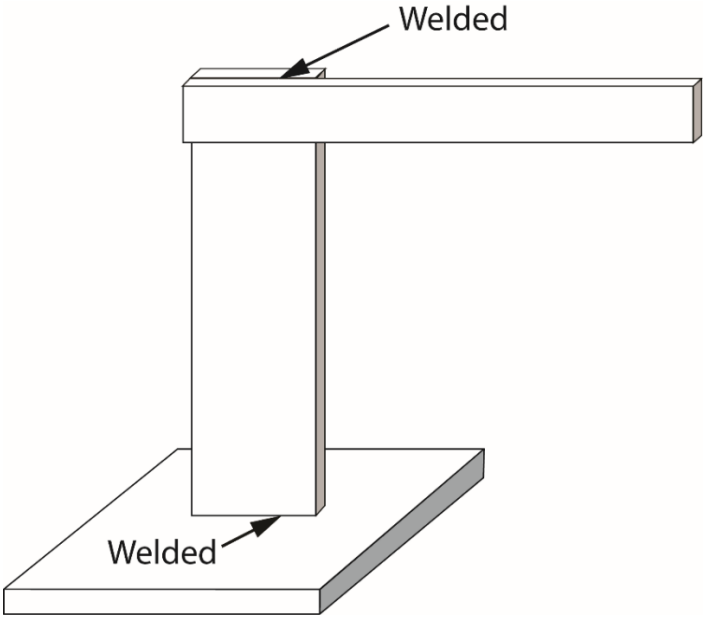

Figure 6-2 Design schematic of flexure

6.2.2 Simulation of Flexure Vibration Modes

The frequency response is designed by observing the results from Solidworks Frequency Simulation. The height, width and thickness of the bars are varied until desired frequencies of the vibration modes have been reached. The two desired vibration modes have to be close in frequency, in counter-phase so that it can mimic the dynamics of a machine tool in counter-phase.

Table 6-1 Flexure dimensions

	Dimension	Value (inches)
Vertical Bar	Length	10
	Width	2
	Thickness	¼
Horizontal Bar	Length	10
	Width	2
	Thickness	¼

The frequency values that Solidworks simulations of the flexure yielded are as seen in Table 6-2. The physical displays of the vibration modes are seen in Figure 6-3 and Figure 6-4, respectively.

Table 6-2 Simulated vibration mode frequencies

Mode Number	Frequency (Hz)
1	48.57
2	107.74

The two modes can seen as in counter-phase from the front view and the top view. The first mode at 48.57 Hz is a pure bending mode in one direction by the vertical bar. The horizontal bar is also bending in the same direction as the vertical bar. The second mode at 107.74 Hz has the vertical column bending in one direction but the horizontal bar bends in the opposite direction. This is the counter-phase mode. The behavior is similar to the counter-phase column and ram behavior as seen in Figure 2-9.

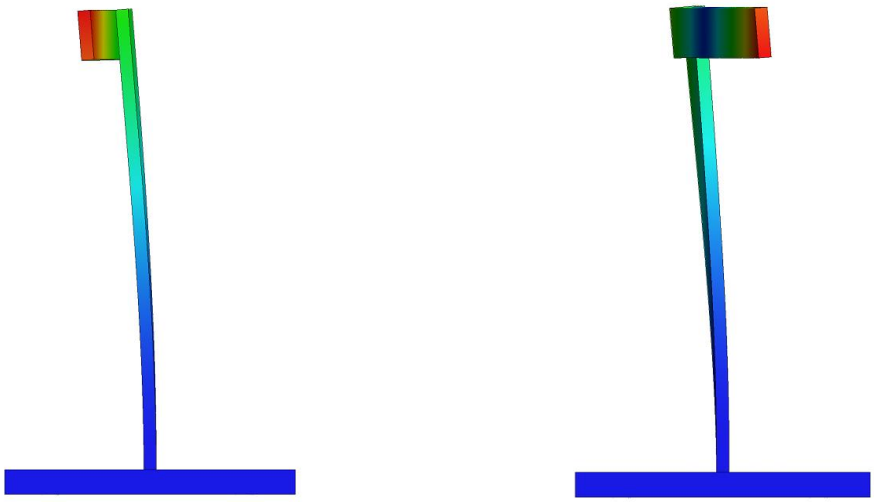

48.75 Hz **107.74 Hz**

Figure 6-3 Simulated vibration modes for flexure (front view)

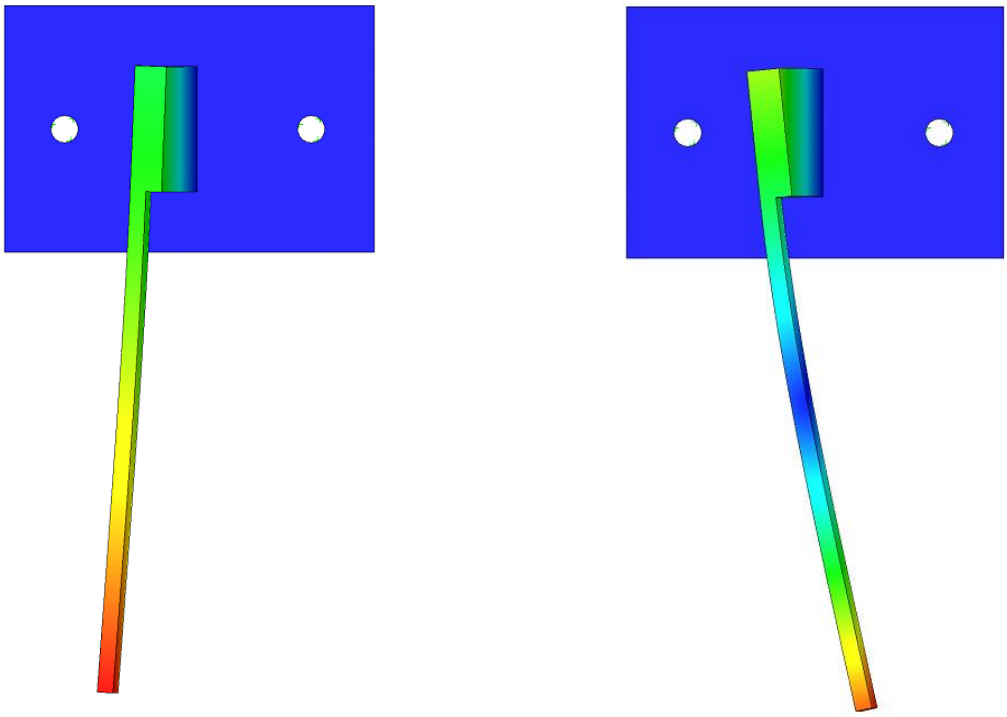

48.75 Hz **107.74 Hz**

Figure 6-4 Simulated vibration modes for flexure (top view)

6.3 Experimental Validation

In order to verify the flexure simulation results of the vibration mode frequencies and its mode shapes, impact hammer testing was performed on the flexure. Roving hammer method was applied. The flexure is clamped down on a granite table to be isolated from other vibration sources.

6.3.1 Counter-phase Verification

The counter-phase mode behavior can be verified by viewing the imaginary portion of the flexure FRF. This can be seen in Figure 6-6. The imaginary magnitude of the two vibration modes are in opposite directions. This implies that the displacement of the flexure at the two frequencies are in opposite directions.

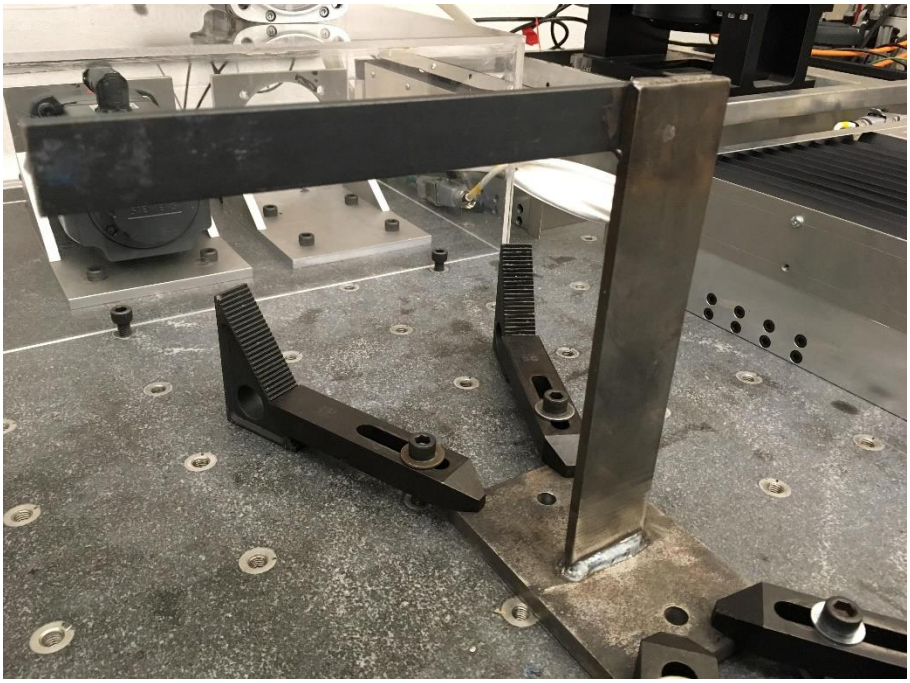

Figure 6-5 Manufactured and assembled flexure

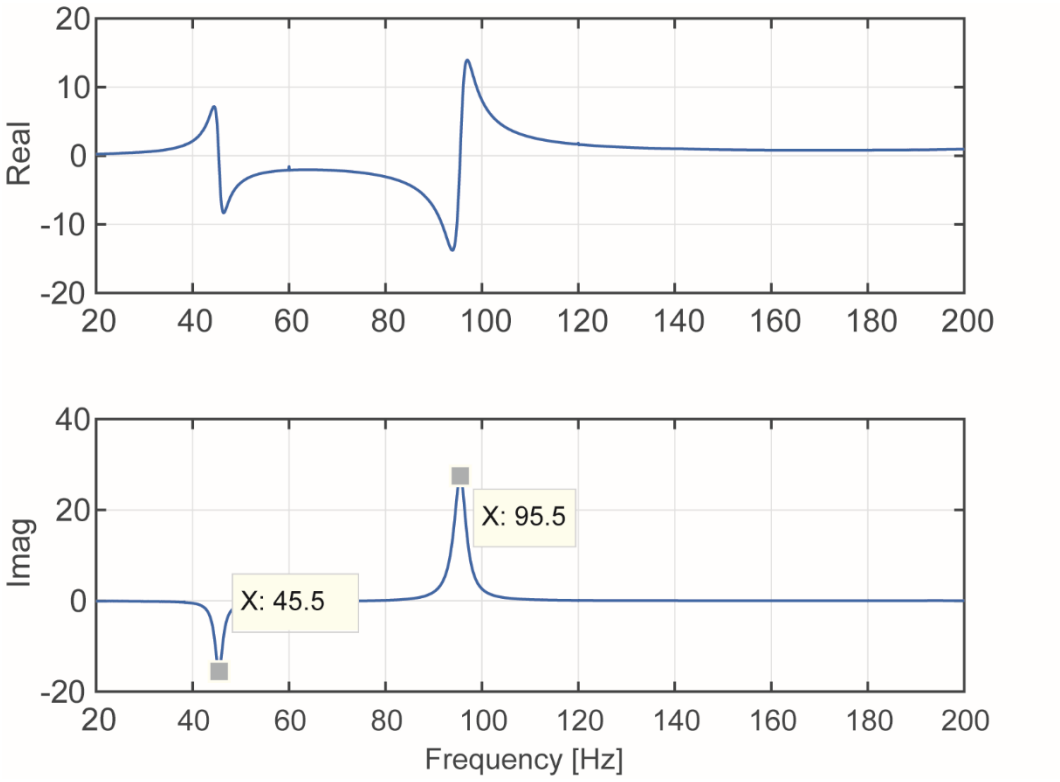

Figure 6-6 Real and imaginary FRF of flexure

6.3.2 Mode Shape Verification

The mode shapes of the flexure are synthesized to ensure that the flexure modal displacements are the same as in the Solidworks simulations. Hammer tap tests will be conducted to obtain the FRFs necessary to create the mode shape drawings. A schematic of the hammer impact location can be seen in Figure 6-7. The green circles indicate the hammer impact locations (input) and the red box indicates the attached accelerometer (output).

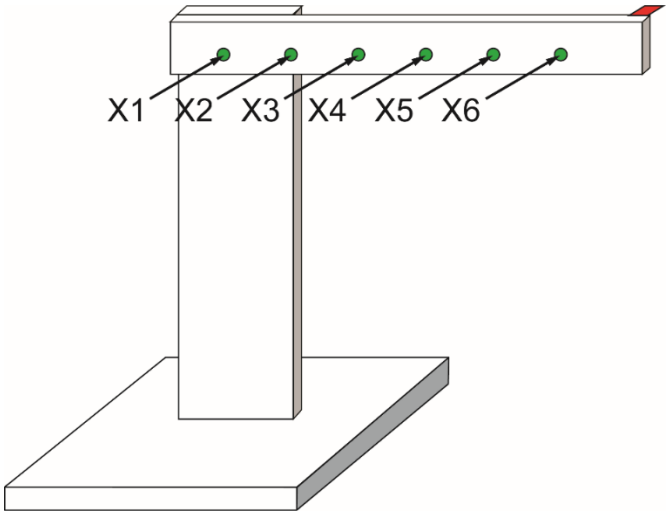

Figure 6-7 Tap test points on flexure

Table 6-3 Sketch of flexure horizontal bar modes from tap test data

Flexure	Mode 1 (46.5 Hz)	Mode 2 (102 Hz)
	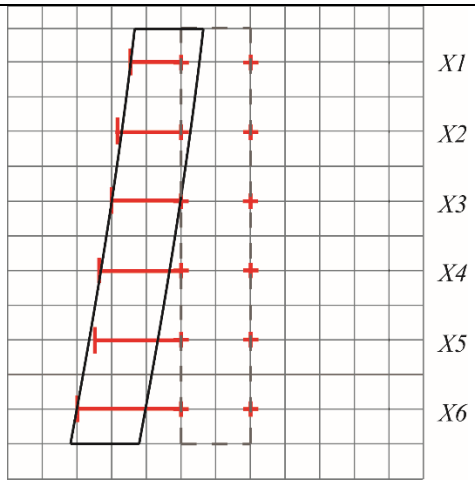	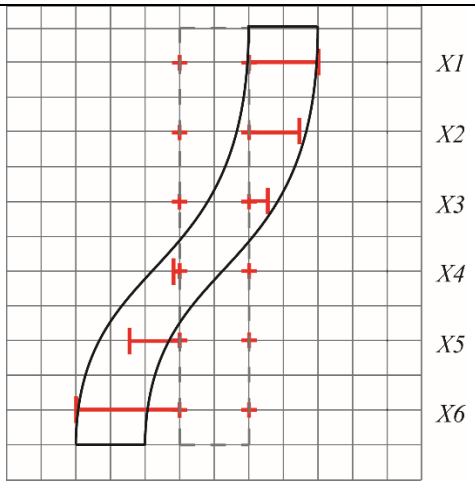

After the natural frequency and damping values have been extracted from FRFs obtained by tap testing, sketches are conducted. As seen from Table 6-3, the values of the simulated modes are very close to the real modes obtained from experimentation. The counter-phase mode behavior can be seen in the second mode.

6.3.3 Model Calculation

The damping ratios of the two modes of the flexure can be found by using the curve-fitting algorithm as described previously in Chapter 5. The fitted model of the FRF can be seen in Figure 6-8 and the model parameters can be seen in Table 6-4.

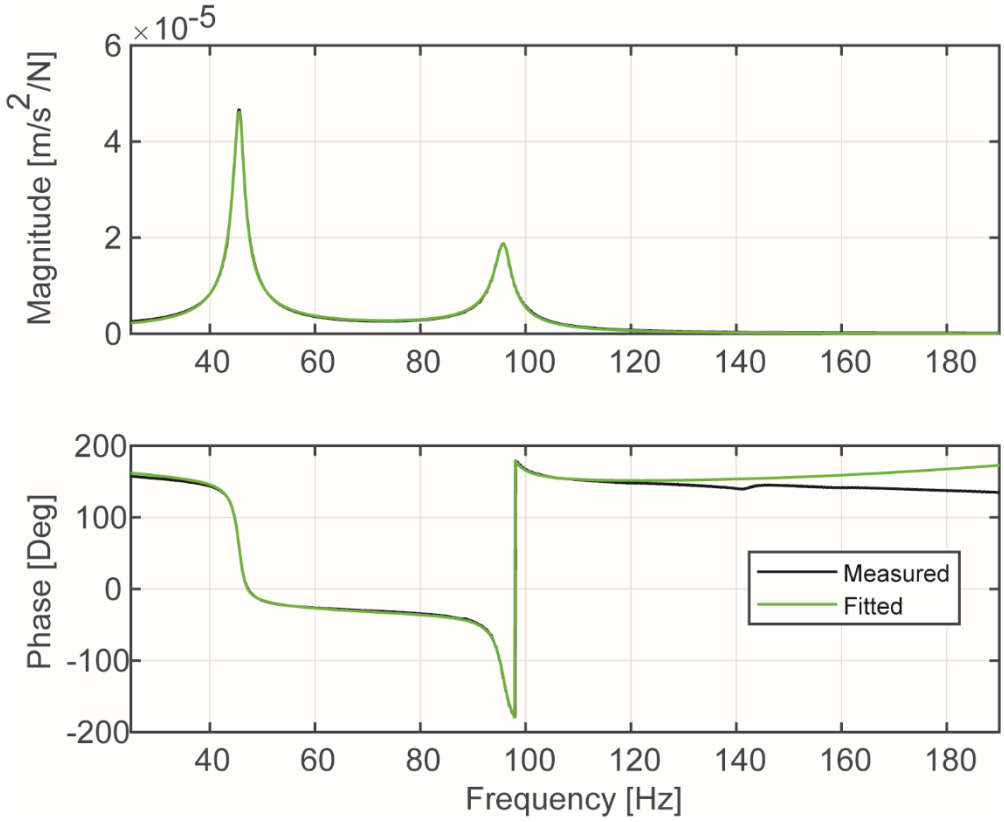

Figure 6-8 Flexure FRF curve fit

Table 6-4 Modal parameters of flexure

Mode	Natural Frequency (Hz)	Damping Ratio
1	45.6531	0.0238
2	95.8730	0.0163

With the flexure verified and its modal parameters identified, the fitted model can now be used in model-based controller design.

6.4 Conclusion

In this chapter, the design of a flexure containing two modes with counter-phase vibration mode behavior is presented. The design process starts with an iterative simulation process in selecting the flexure dimensions and geometry to obtain the desired frequency responses. The simulated results is verified against experimental results using the roving tap testing method and obtaining a FRF from the flexure. The modes are then hand sketched to verify the mode shapes. The modal synthesis method is used to extract natural frequency and damping values. The flexure will be used for model-based controller synthesis in Chapter 7 where the counter-phase vibration modes will be suppressed.

Chapter 7
$\mathcal{H}_\infty$ and $\mathcal{H}_2$ Model-Based Controller Design

7.1 Introduction

In this chapter, the use of $\mathcal{H}_\infty$ and $\mathcal{H}_2$ optimal regulation theory for robust control system design is introduced. Model-based controllers such as $\mathcal{H}_\infty$ and $\mathcal{H}_2$ controller design is aimed to achieve good disturbance rejection and guarantee stability and robustness of the system response [31] [32]. An advantage of using this synthesis technique is that there is no need to separately design an observer and controller. The $\mathcal{H}_\infty$ and $\mathcal{H}_2$ synthesis algorithms designs both the observer and controller simultaneously. A challenge of controller design is to select the weightings that best achieve the performance desired.

In this chapter, a way of specifying the weights on the desired closed-loop transfer function to suppress vibrations is introduced. $\mathcal{H}_\infty$ and $\mathcal{H}_2$ controllers are created, tested in simulation and experimentation. The weight selection steps is explained in Section 7.2. Experimental results and comparisons are presented in Section 7.3.

7.2 Mixed Sensitivity Controller Synthesis

Mixed sensitivity $\mathcal{H}_\infty$ and $\mathcal{H}_2$ controller synthesis use defined weighting functions to shape the sensitivity function of the closed-loop system to achieve desired system performances and robustness [33]. A system block diagram can be seen in Figure 7-1. The primary objective of the controllers is to minimize the impact of disturbances on the system.

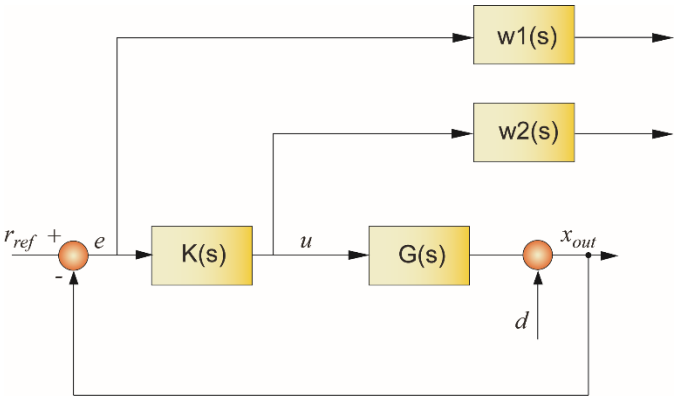

Figure 7-1 Augmented closed-loop system with controller [33]

The plant is represented by $G(s)$ and the controller is represented by $K(s)$. The signal d represents the disturbances to the system, r as the reference signal, which is typically zero, and x is the measured output. The two weights W_1 and W_2 are the sensitivity weighting function and controller weighting function, respectively.

7.2.1 Sensitivity Weighting

The sensitivity function is directly related to the closed-loop disturbance. The active damping control loop diagram can be seen in Figure 7-2. The open-loop disturbance transfer function can be modeled just by the dynamics of the structure (G_{a1f1}) because the system reference input is zero. The closed-loop disturbance transfer function can be calculated by multiplying the sensitivity of the system by the open-loop disturbance transfer function as seen in Eqn. (7.1). The sensitivity function is formulated as the closed-loop transfer function from the disturbance to the output **[32]**. Thus, the closed-loop disturbance can be directly shaped by the sensitivity function.

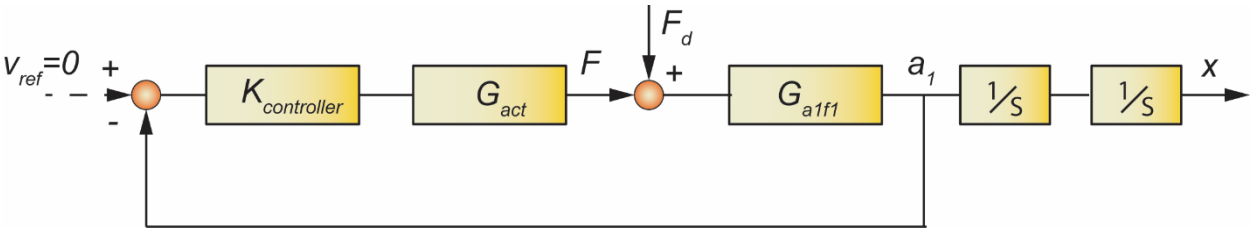

Figure 7-2 System control loop diagram for active damping

$$G_d^{closed-loop} = S \cdot G_{a1f1} = S \cdot G_d \tag{7.1}$$

$$G_d^{closed-loop} = \frac{1}{1 + G_{act} \cdot G_d \cdot K} \cdot G_d \tag{7.2}$$

$$\max_{for\ all\ \omega} |S(j\omega)| \leq |W_1^{-1}(j\omega)| \tag{7.3}$$

From Eqn. (7.2) it can be seen that the controller directly affects the sensitivity, which in turn affects the closed-loop disturbance. A weighting function $|W_1^{-1}(j\omega)|$ can be used in the mixed-sensitivity controller synthesis algorithm to shape the sensitivity as seen by Eqn. (7.3) **[33]**. An example of this approach can be seen in Figure 7-3 where a weighting function W_p is used to synthesis a controller to suppress the peak of the sensitivity function S.

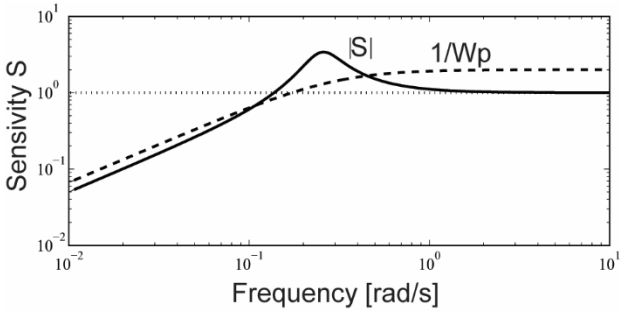

Figure 7-3 Sensitivity shaping function [32]

7.2.2 Controller Input Weighting

The controller input weighting function determines the control effort. It is currently set to a constant value. The weighting is to limit the amount of controller force the synthesized controller will have. The user specifies this value and adjusts the value based on the observed simulated outputs to maximize vibration suppression, minimize controller effort and avoid actuator saturation. The specification for the controller input can be seen in Eqn. (7.4) [33].

$$\max_{for\ all\ \omega} |R(j\omega)| \leq |W_2^{-1}(j\omega)| \tag{7.4}$$

7.2.3 Controller Synthesis

The MATLAB functions *augw*, *hinfsyn* and *h2syn* are used to synthesize the model-based controllers. The *augw* function augments the state-space model by incorporating the sensitivity and controller weighting functions. The *hinfsyn* and *h2syn* functions will the compute the optimal controllers based on the augmented system model with the performance weighting functions. The $\mathcal{H}_\infty$ and $\mathcal{H}_2$ algorithm for incorporating the weighting function specifications can be seen in Eqn. (7.5) [33].

$$\left\| \begin{matrix} W_1(j\omega)S(j\omega) \\ W_2(j\omega)R(j\omega) \end{matrix} \right\|_{\infty,2} < 1 \tag{7.5}$$

The targets of the $\mathcal{H}_\infty$ and $\mathcal{H}_2$ controllers can be seen in Figure 7-4. The $\mathcal{H}_\infty$ aims to minimize the ∞-norm (maximum peak) of the function. The $\mathcal{H}_2$ controller aims to minimize the 2-norm (area underneath) of the function.

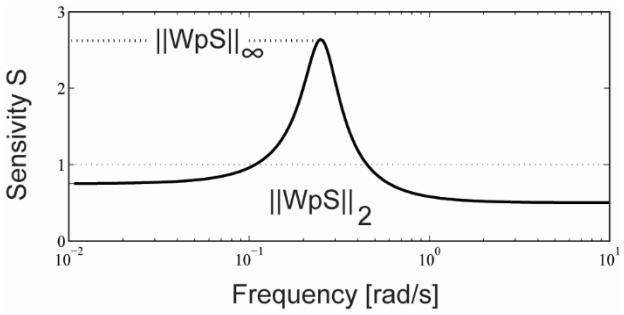

Figure 7-4 $\mathcal{H}_\infty$ and $\mathcal{H}_2$ norms on sensitivity function [32]

7.3 Experimental Validation

To test the $\mathcal{H}_\infty$ and $\mathcal{H}_2$ controllers, a Modal Shop 2075E shaker is mounted on the custom built flexure as described in Chapter 6. This can be seen in Figure 7-5. The shaker is connected to the flexure through a stringer, PCB 208C02 force sensor and a magnet to keep the stinger attached to the flexure. The shaker will be used as a structural exciter and vibration damping actuator. A PCB accelerometer is attached to the tip of the flexure for sensing the disturbances and for feedback control. The shaker and accelerometer are connected to a dSPACE data acquisition and controller hardware. The control signal will be sent out by the dSPACE hardware. A hammer tap test will be used to capture the closed-loop response of the system. The flexure will be excited by the hammer and the resulting closed-loop FRF will be captured by the accelerometer. The modal analysis software Cutpro will be used to capture the FRFs.

7.3.1 Weight Selection

The sensitivity weighting function is selected from the open-loop FRF of the flexure, which represents disturbance transfer function of the flexure. The curve fitted model from the open-loop FRF is used for the controller synthesis. The sensitivity weighting function is normalized by the ∞-norm and 2-norm for the respective controller synthesis to have a common scale factor. This would make controller tuning work for systems with different orders of magnitude. The weighting function is also in series with second ordered high and low pass filters to attenuate noise and any unwanted contributions to the weightings out of the frequency range of interest. The weighting function can be seen in Eqn. (7.6). The controller weighting function is defined as a constant value to increase or decrease the control effort.

$$W_1 = \frac{G_d}{\|G_d\|_{\infty,2}} F \tag{7.6}$$

$$W_2 = Constant \tag{7.7}$$

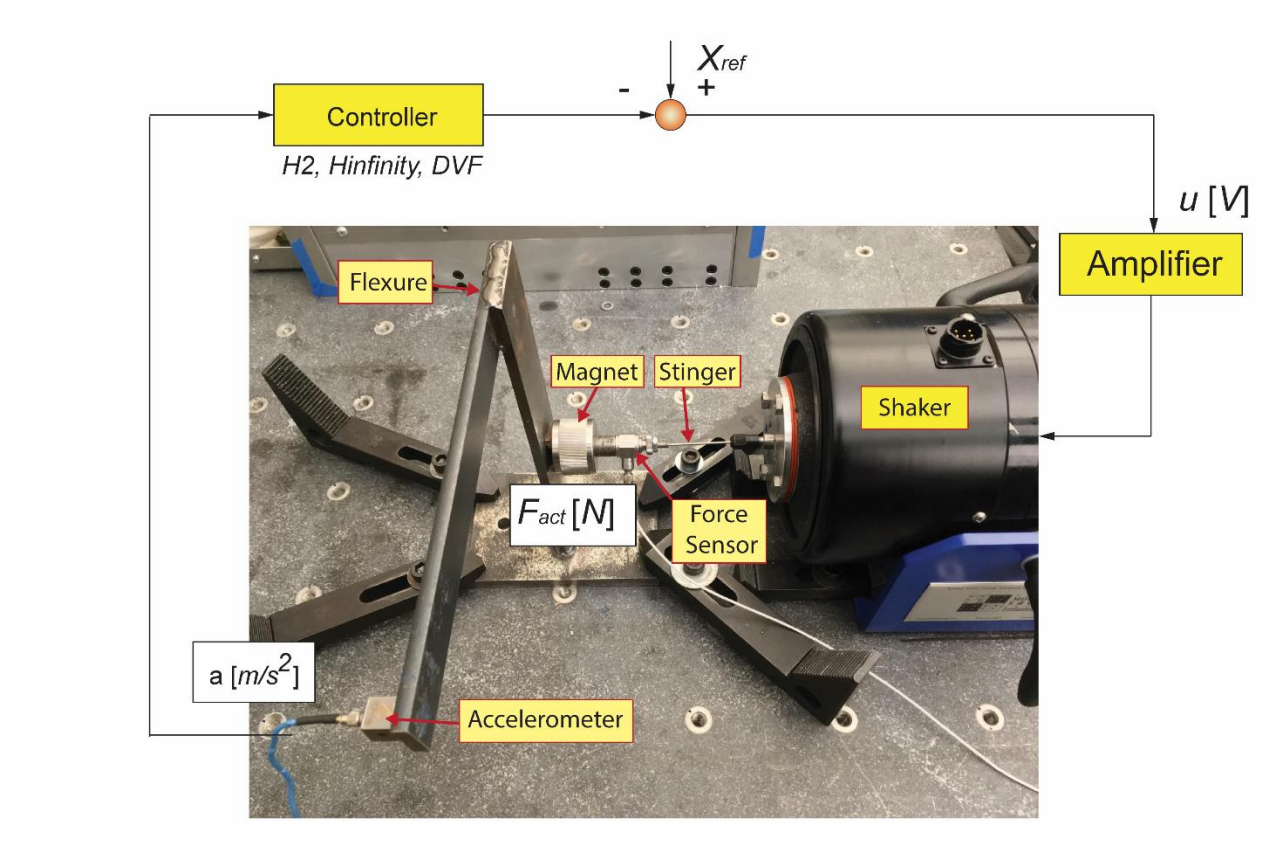

Figure 7-5 Experimental setup for active damping of flexure vibration modes

7.3.2 Controller Parameter Tuning

The values of the filters and controller parameters are tuned by using the prediction tool as described previously in Chapter 4. The vibration mode suppression is maximized by iterating through the controller parameter values while to minimize the vibration peaks within the closed-loop FRF. The system model is identified as a 4th order model using the curve-fitting algorithm. The model-based controllers are reduced to a 4th order controller after synthesis to better compare against the 4th order DVF controller. Balanced truncation method is used to reduce the controller order [34]. Sampling time is set to be 4 kHz. The sensitivity function and controller is monitored to ensure that controller does not destabilize modes at other frequencies and that the controller does not saturate. Stability is monitored by viewing the Nyquist plot. The final controller parameter values can be found in Table 7-1. The control loop can be seen in Figure 7-5.

Table 7-1 Controller parameters values

Controller Parameter	Direct Velocity	$\mathcal{H}_\infty$	$\mathcal{H}_2$
Gain	-750	-1	-1
Low Pass	62 Hz	120 Hz	120
High Pass	29 Hz	20 Hz	20
Improvement Factor	-	0.05	0.01

7.3.3 Results

The following section shows the comparison of the different results from each of the controllers. Firstly, a comparison between the simulated and measured closed-loop FRFs of the flexure can be seen in Figure 7-6. The dashed line represents the predicated closed-loop FRF and the solid line represents the measured FRF. The measured FRF is obtained with hammer impact testing. The data is measured by using CutPRO software and a PCB Electronics impact hammer. It can be seen that the prediction is quite accurate as there is little deviation between the predicted closed-loop response and the measured response both in magnitude and in phase.

The suppression of the vibration modes using the model-based controllers are quite effective. The results can be viewed in Figure 7-7. The $\mathcal{H}_2$ controller is able to suppress 80% of the first vibration mode and 63% of the second mode. Its sensitivity and the controller gain are both able to be maintained under two. The $\mathcal{H}_\infty$ controller is able to suppress the first mode even more than the $\mathcal{H}_2$ controller with a reduction of 85% but it is only able to damp 39% the second mode. This is because the $\mathcal{H}_\infty$ controller minimizes the highest peak of the FRF (∞-norm) whereas the $\mathcal{H}_2$ controller minimizes the area underneath the FRF (2-norm). The $\mathcal{H}_\infty$controller gains and sensitivity values are higher at frequencies above 100 Hz. This can be attributed to the noise within the hammer tap test measurement and due to the optimization technique. All of the controllers were stable using the Nyquist stability criterion.

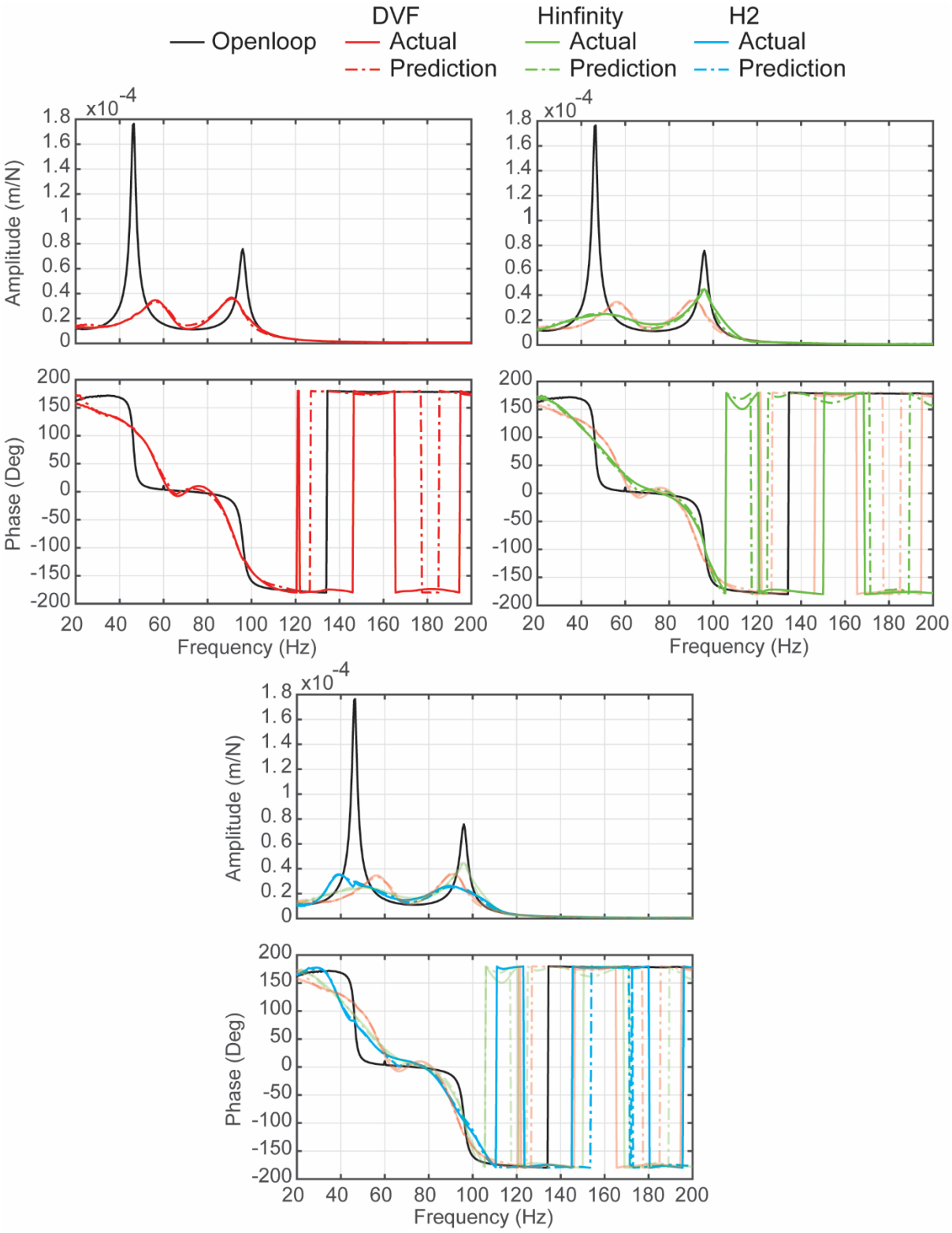

Figure 7-6 Simulated versus predicted FRFs

However, the dynamics of the flexure is found to be too simple. The DVF controller is able to damp the second mode as well by placing the low pass filter at 62 Hz. There is a shift of the vibration modes in frequency as well. The first mode shifts from 46 Hz to 56 Hz and the second mode shifts from 95.5 Hz to 90.5 Hz. The first mode is reduced by 81% and the second mode is reduced by 52%. The sensitivity function of the DVF controller is higher than the sensitivity function of the $\mathcal{H}_\infty$ and $\mathcal{H}_2$ controllers. The controller gain of the DVF controller is higher than the $\mathcal{H}_2$ controller. This implies that the DVF controller requires more force to achieve the damping.

A summary of the reduction effects can be found in Table 7-2. The magnitudes and the percentage reduction of the vibration modes are shown.

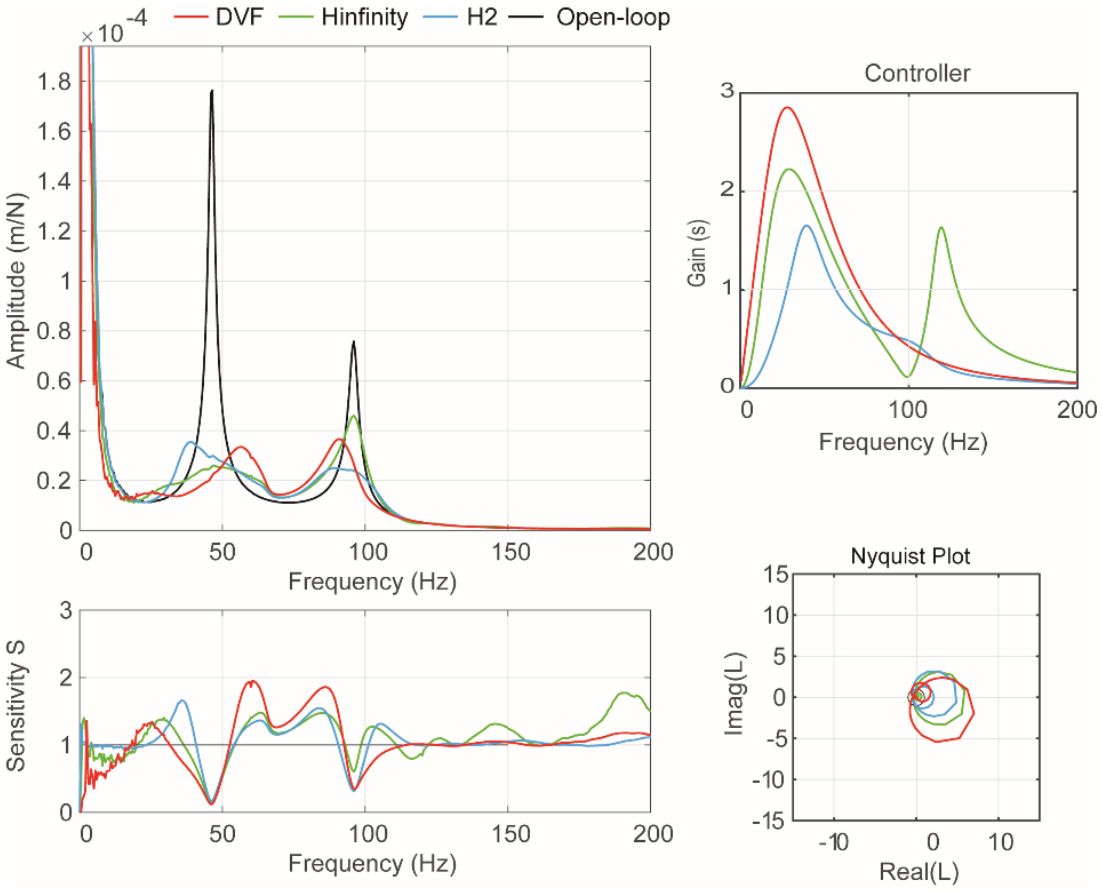

Figure 7-7 Closed-loop response controller tuning window

Table 7-2 Magnitude and percentage reduction of vibration modes with controllers

Controller	Mode 1		Mode 2	
	Magnitude Before	1.763e-4	**Magnitude Before**	7.576e-5
	Magnitude (m/N)	**Reduction (%)**	**Magnitude (m/N)**	**Reduction (%)**
DVF	4.965e-5	81	3.656e-5	52
$\mathcal{H}_\infty$	3.54e-5	85	4.593e-5	39
$\mathcal{H}_2$	2.607e-5	80	2.429e-5	63

The original intent of the flexure is to mimic the dynamics of the ram-type machining center as seen in Figure 2-9. The machine's drives were used to damp the machine ram dynamics in a non-collocated control. Model-free controllers such as DVF and DAF were not able to damp the complex dynamics of the machine. The counter-phase mode behavior observed in the machining center would be an ideal situation to implement the model-based controls. With the development of the model-based controller tuning technique and tools, non-collocated controls for vibration damping can be implemented on machine tools with complex dynamics.

7.4 Conclusion

In this chapter, a synthesis technique for the model-based $\mathcal{H}_\infty$ and $\mathcal{H}_2$ controller is introduced. The technique is aimed at the application of active vibration damping of machine tools and workpieces with counter-phase modes. Model-free controllers such as DVF and DAF are not able to suppress counter-phase vibration modes in machine tools with complex dynamics. A flexure designed with two vibrations modes as previously introduced in Chapter 6 is mounted on a granite table attached with a shaker actuator. The actuator is used for damping the vibration modes in the flexure. Both model-based controllers were able to suppress the vibration modes of the flexure. Due to the simple dynamics of the flexure, a DVF controller is able to suppress the flexure dynamics even though it is in counter-phase. The $\mathcal{H}_2$ controller is found to have the best vibration suppression using the minimal control effort. The model-based controller should be continued to be tested on machine tools or workpieces with vibration modes in counter-phase to observe its robustness.

Chapter 8
Conclusions and Future Work

8.1 Conclusion

In this thesis, two methods of synthesizing and optimizing controllers to suppress vibration disturbances using inertial actuators are presented. A frequency domain based algorithm to determine the optimal closed-loop controller for an actuator to suppress the vibration modes of a machine tool or workpiece is introduced. Ranges of controller values are iterated upon to find the optimal controller values. A prediction of the closed-loop response is made for each controller combination. An objective function is calculated based on the area underneath the FRF. The controller value that achieves the minimal objective function will exhibit the maximum suppression of vibration modes. Stability of the system is monitored through the Nyquist plot. User defined sensitivity constraints are monitored as well to prevent actuator saturation and adequate noise suppression. The algorithm has been experimentally verified on a Soraluce machining center and on a workpiece with an attached actuator.

However, the DVF controller used for autotuning does not work for all machining situations. In the case of counter-phase modes, one mode is damped and the other mode is destabilized. This introduces the need for model-based controls. Model-based controls creates a model of the system from the obtained data and synthesizes a controller based on the model created and performance requirements. A least squares based curve-fitting algorithm is created in order to derive a model from the obtained FRF. The user picks the frequency range and the frequencies of the vibration modes that they would like to fit. The data range used to form the regressor matrix is found by using the mobility Nyquist plot of each user selected vibration mode. A small set of data points is used first to form a circle that represents the Nyquist circle The data range is extended from the small set until the data points are no longer within the formed circle. The data range for each vibration mode is used in the least squares problem to extract its respective natural frequency and damping ratio value. The accumulation of the natural frequencies, damping ratios and its residual terms of the vibration modes make up the model of the system.

A flexure is developed in order to test the model-based controller designs. A flexure is designed using CAD software to ensure that the vibration modes exhibit counter-phase behavior. The vibration mode frequencies are experimentally verified by obtaining FRFs through roving hammer tap testing. The flexure mode shapes are drawn from the obtained FRFs from hammer tap testing to ensure the flexure

displacements match the CAD simulations. Modes at 45.5 and 95.5 Hz have been identified, which are close to the simulated values of 48.75 Hz and 107.74 Hz respectively.

The $\mathcal{H}_\infty$ and $\mathcal{H}_2$ model-based controllers are implemented on the counter-phase mode flexure using an external actuator after its model has been identified. The resultant FRF is obtained through hammer testing. The resultant FRFs are compared against the optimal DVF controllers. It is seen that the $\mathcal{H}_\infty$ and $\mathcal{H}_2$ controllers are able to successfully suppress both vibration modes of the flexure. However, after additional analysis and tuning of filters, the DVF method is found to able to damp the counter-phase vibrations as well. This is due to the simple dynamics of the flexure which allows the DVF controller to still work. In the future, the model-based controller will be tested on a machine or workpiece with more counter-phase modes where the DVF controller fails.

8.2 Future Work

The future work of this project is to conduct further work and research into vibration damping controls during machining. The frequency based autotuning algorithm should be implemented on more workpieces with the portable actuator to ensure that it is robust enough for all machining situations. The $\mathcal{H}_\infty$ and $\mathcal{H}_2$ controllers are verified on a lab setting but have not been verified during a machining process. In the future, the controllers will be tested on Soraluce milling machines at IK4-Ideko where the system dynamics are more complex and possess more vibration modes in counter-phase.

Bibliography

[1] M. Siddhpura and R. Paurobally, "A review of chatter vibration research in turning," *International Journal of Machine Tools & Manufacture,* vol. 61, no. 1, pp. 27-47, 2012.

[2] J. Munoa, X. Beudaert, Z. Dombovari, Y. Altintas, E. Budak and C. Brecher, "Chatter suppression techniques in metal cutting," *CIRP Annals - Manufacturing Technology,* vol. 65, no. 2, pp. 785-808, 2016.

[3] J. Munoa, X. Beudaert, K. Erkorkmaz, A. Iglesias, A. Barrios and M. Zatarain, "Active suppression of stuructural chatter vibrations using machine drives and accelerometers," *CIRP Annals - Manufacturing Technology,* vol. 64, no. 1, pp. 385-388, 2015.

[4] Y. Altintas and M. Weck, "Chatter Stability of Metal Cutting and Grinding," *CIRP Annals,* vol. 53, no. 2, pp. 619-642, 2004.

[5] J. Munoa , I. Mancisidor, N. Loix, L. Uriarte, R. Barcena and M. Zatarain , "Chatter suppression in ram type travelling column milling machines using a biaxial inertial actuator," *CIRP Annals - Manufacturing Technology,* vol. 62, no. 1, pp. 407-410, 2013.

[6] Y. Altintas, Manufacturing Automation, Cambridge: Cambridge University Press, 2000.

[7] S. Tobias, Machine Tool Vibration, Blackie and Sons Ltd., 1965.

[8] F. Koenigsberger and J. Tlusty , Machine Tool Structures-Vol. I: Stability Against Chatter, Pergamon Press., 1967.

[9] Y. Altintas and J. Ko, "Chatter Stability of Plunge Milling," *CIRP Annals,* vol. 1, no. 55, pp. 361-364, 2006.

[10] E. Budak and Y. Altintas, "Analytical Prediction of Stability Lobes in Milling," *CIRP Annals,* vol. 44, no. 1, pp. 357-362, 1995.

[11] Y. Altintas and E. Budak, "Analytical Prediction of Stability Lobes in Milling," *CIRP Annals,* vol. 44, no. 1, pp. 357-362, 1995.

[12] E. Budak and Y. Altintas, "Prediction of Milling Force Coefficients from Orthogonal Cutting Data," *Journal of Manufacturing Science & Engineering,* vol. 118, no. 1, pp. 216-224, 1996.

[13] I. Mancisidor Aizpurua, Active chatter suppression by means of computer-controlled inertial actuators, Bilbao: School of Industrial Technical Engineering of Bilbao, 2014.

[14] Y. Altintas and P. Chan, "In-process Detection and Suppression of Chatter in Milling," *International Journal of Machine Tools Manufacturing,* vol. 32, no. 3, pp. 329-347, 1992.

[15] Y. Altintas, S. Engin and E. Budak, "Analytical Stability Prediction and Design of Variable Pitch Cutters," *Journal of Manufacturing Science and Engineering,* vol. 121, no. 1, pp. 173-178, 1999.

[16] T. Insperger and G. Stepan, "Stability Analysis of Turning With Periodic Spindle Speed Modulation Via Semidiscretization," *Journal of Vibration and Control,* vol. 10, no. 12, pp. 1835-1855, 2004.

[17] J. Alvarez, M. Zatarain and D. Barrenetxea, "Semi-discretization for Stability Analysis of In-feed Cylindrical Grinding with Continuous Workpiece Speed Variaction," *International Journal of Advanced Manufacturing Technology,* vol. 69, no. 1, pp. 113-120, 2013.

[18] I. Inasaki, B. Karpuschewski and H. Lee, "Grinding Chatter – Origin and Suppression," *CIRP Annals,* vol. 50, no. 2, pp. 515-534, 2001.

[19] C. Brecher, S. Baumler and B. Brockmann, "Avoiding Chatter by Means of Active Damping Systems for Machine Tools," *Journal of Machine Engineering,* vol. 13, no. 3, pp. 117-128, 2013.

[20] B. Chung, S. Smith and J. Tlusty, "Active Damping of Structural Modes in High-Speed Machine Tools," *Journal of Vibration and Control,* vol. 3, no. 3, pp. 279-295, 1997.

[21] C. Brecher and M. Week , "Electrohydraulic Active Damping System," *CIRP Annals,* vol. 54, no. 1, pp. 389-392, 2005.

[22] M. Zaeh, R. Kelinwort, P. Fagerer and Y. Altintas , "Automatic tuning of active vibration control systems using inertial actuators," *CIRP Annals - Manufacturing Technology,* vol. 66, no. 1, pp. 365-368, 2017.

[23] B. Chaudhuri, C. P. Bikash, A. Zolotas, I. Jaimoukha and T. Green, "Mixed-Sensitivity Approach to H Control of Power System Oscillations Employing Multple FACTS Devices," *IEEE Transactions on Power Systems,* vol. 18, no. 3, pp. 1149-1156, 2003.

[24] M. Klein, L. Le, G. Rogers, S. Farrokhpay and N. Balu, "H Damping Controller Design in Large Power Systems," *IEEE Transactions on Power Systems,* vol. 10, no. 1, pp. 158-166, 1995.

[25] X. Beudaert, A. Barrios, K. Erkorkmaz and J. Munoa, "Limiting factors for the active suppression of structural chatter vibrations using the machine's drives," in *XIIth International Conference of High Speed Machining,* Nanjing,China, 2015.

[26] D. Ewins, Modal Testing: Theroy, Practice and Application, Philadelphia: Research Studies Press Ltd., 2000.

[27] N. Loix and J. Verschueren, "Stand-alone active damping device," in *9th International conference on new actuators*, Bermen, Germany, 2004.

[28] Siemens, "Siemens PLM Community," Siemens, 11 07 2016. [Online]. Available: https://community.plm.automation.siemens.com/t5/Testing-Knowledge-Base/What-modal-impact-hammer-tip-should-I-use/ta-p/355026. [Accessed 19 11 2018].

[29] G. Franklin, D. Powell and A. Emami-Naeini, Feedback control of dynamic systems. Fifth edition, Upper Salle River, New Jersey: Pearson Prentice Hall, 2006.

[30] A. Ozedemir and S. Gumussoy, "Transfer function estimation in system identification toolbox via vector fitting," in *Proceedings of the 20th World Congress of the International Federation of Automatic Control*, Toulouse, France, 2017.

[31] H. Kwakernaak, "Robust control and Hinfinity optimization - Tutorial paper," *Automatica*, vol. 29, no. 2, pp. 255-273, 1993.

[32] I. Postlethewaite and S. Skogestad, Multivariable Feedback Control: Analysis and Design, England: J. Wiley, 2007.

[33] H. Kwakernaak, "Mixed Sensitivity Design," in *15th IFAC World Congress*, Barcelona, Spain, 2002.

[34] A. Varga, "Balancing-free square-root algorithm for computing singular pertubation approximations," in *30th IEEE CDC*, Brighton, UK, 1991.

Appendix A

Table A-1 Model parameters of production box workpiece curve fit

Selected Modes							
Proposed					MATLAB Modalfit		
Mode	**ω_n**	**ζ_n**	**α_k**	**β_k**	**Mode**	**ω_n [rad/s]**	**ζ_n**
1	244.00	0.0095	322.69	-0.9449	1	241.61	0.0488
2	300.99	0.0033	90.26	-0.1401	2	298.45	0.0036
3	440.08	0.0041	-98.50	0.2073	3	491.17	0.0304
4	494.34	0.0173	2414.21	-8.8834	4	578.27	0.0209
5	582.27	0.0126	748.59	-7.1382	5	695.03	0.0336
6	704.16	0.0197	-901.26	-42.4624	6	720.00	0.0116
7	717.01	0.0076	7458.97	19.8333	7	785.36	0.0092
8	714.09	0.0058	5510.04	-13.0706	8	856.61	0.0073
9	786.46	0.0086	13935.28	-15.0314	9	973.58	0.0059
10	857.00	0.0073	24285.61	-29.1880	10	1008.59	0.0249
11	970.45	0.0056	4346.07	-4.2991	11	1032.12	0.0069
12	1030.89	0.0073	21355.94	-46.3609	12	1152.37	0.0037
13	1812.44	0.0010	1572.92	-13.5251	13	1284.36	0.0018
14	1781.67	0.0003	1106.88	-1.1618	14	1386.42	0.0055
15	1879.02	0.0010	-3383.68	-3.3336	15	1493.69	0.0116
16	1924.42	0.0019	-13776.15	-9.3845	16	1578.71	0.0024
17	1987.57	0.0029	28085.78	-61.7018	17	1781.54	0.0040
18	2042.87	0.0032	-15426.30	-14.8007	18	1812.03	0.0014
19	2204.00	0.0024	427095.49	27.3664	19	1846.52	0.0013
Residual Components					20	1877.07	0.0030
1	2204.75	0.0022	-449676.99	-8.7133	21	1893.55	0.1835
2	2133.65	0.0015	4977.06	-4.2531	22	1922.51	0.0028
3	2076.06	0.0070	-11411.15	-4.8434	23	1983.26	0.0006
4	1985.91	0.0019	-29221.86	-0.0520	24	1987.58	0.0034
5	1909.49	0.0010	5348.52	-0.1218	25	1990.45	0.0006

6	1871.84	0.0051	1797.09	-7.6660	26	2014.47	0.0014
7	1773.88	0.0059	25383.53	-8.0695	27	2038.69	0.0050
8	1578.01	0.0031	2975.04	-2.2417	28	2140.54	0.0023
9	1386.82	0.0068	6142.41	-5.1174	-	-	-
10	1284.87	0.0029	2321.30	-3.9389	-	-	-
11	1078.81	0.3633	-43711.94	-310.2130	-	-	-
12	1027.20	0.0067	-11646.37	6.3883	-	-	-
13	998.35	0.0164	9858.75	10.5091	-	-	-
14	896.93	0.0320	-2591.73	5.6879	-	-	-
15	793.52	0.0049	818.32	0.5260	-	-	-
16	633.15	0.0110	-1741.68	1.5871	-	-	-
17	430.28	0.0431	75.67	3.3321	-	-	-
18	254.94	0.0530	1588.64	-1.9444	-	-	-